www.geo-gsnl.org

Virunga Volcanoes Supersite Biennial Report: 2022- 2023

History	***http://geo-gsnl.org/supersites/permanent-supersites/virunga-supersite/***
Supersite Coordinator	*Charles Balagizi* *Goma Volcano Observatory* *142, Avenue du Rond-Point,* *Quartier des Volcans,* *Goma City, Democratic Republic of the Congo* *Email: balagizi.charles@gmail.com* *Cell : +243 975803568*

1. Abstract

For 2022 and 2023, the activity at Nyiragongo volcano has almost been at background level after the May 2021 eruption. The effusive activity that resumed inside the Nyiragongo main crater in September 2021 began with a sustained seismic activity and ground deformation to the southern flank of the volcano, has shown regular activity with lava presence in the crater captured several times by satellite when weather conditions allow. The degassing is permanent, in fact the two DOAS stations installed around Nyiragongo volcano (one in Rusayo and the other in Sake) indicate that the plume is permanent with 2943 tons/day as maximum daily flux for 2023 and a 300 kt as cumulative SO_2 emissions for 2023, from the DOAS that measures only during the presence of sunlight. It has been challenging to access Nyiragongo summit, the May 2021 eruptive site and the lower parts of Nyiragongo volcano (e.g. for measuring temperature and gas in fractures) because of the ongoing war in the volcanic field, which has even prevented the UN helicopter to overflowing the volcanic field in support to the monitoring activities.

Unlike Nyiragongo volcano, Nyamulagira volcano has been characterized by an intense activity inside its large caldera (~2,2x2 km wide), and as for Nyiragongo, Nyamulagira was not accessible for ground-based measurement or helicopter overflowing because of the security issues. The satellite-based monitoring has played an important role in responding to several unrests recorded during 2023 to 2023, especially in May, June and November 2023 when lava overflowed Nyamulagira's caldera rim. Few local scientists are involved in the processing of the EO data, raison why there is still need to continue improving local capacities to process the EO data and for they interpretation. Discussions have been initiated for the capacities exchange between local and international members of the Supersite.

Considering the fact that gases dissolved in the deep waters of Lake Kivu represent a real hazard for the millions of the populations living in its watershed especially those in the cities of Goma (DRC) and Gisenyi (Rwanda), efforts have been made for the studding the stability of this lake and how could a volcanic eruption and/or the movement of the western branch of the rift where the lake lies could affect its stability. Hence, studies on the imaging of the details of the crustal and the upper mantle structure along the Kivu Rift zone particularly the lake Kivu basin as well on the geochemical monitoring of Lake Kivu are ongoing.

Finally, several local scientists had the opportunity to participate in abroad trainings related to volcano monitoring, as well as volcanic and climatic hazards assessment and mitigation. The Goma Volcano Observatory has also received a donation of 5 GNSS stations from the GEO-GNSL, under the Virunga Supersite umbrella, to improve local infrastructures for a better ground-based collection.

2. Scientists/science teams

Charles M. Balagizi	***Geochemistry Department,*** ***Goma Volcano Observatory. 142, Avenue du Rond-Point, Quartier des Volcans, Goma City, Democratic Republic of the Congo*** ***balagizi.charles@gmail.com*** ***https://www.researchgate.net/profile/Charles_Balagizi***
Georges Mavonga	*Department of Seismology, Goma Volcano Observatory* *142, Avenue du Rond-Point, Quartier des Volcans, Goma City,* *Democratic Republic of the Congo* *mavotulu@gmail.com*
Albert Kyambikwa	*Department of Seismology, Goma Volcano Observatory* *142, Avenue du Rond-Point, Quartier des Volcans, Goma City,* *Democratic Republic of the Congo* *albertuskabi@gmail.com*
Arsène T. Sadiki	*Department of Seismology, Goma Volcano Observatory* *142, Avenue du Rond-Point, Quartier des Volcans, Goma City,* *Democratic Republic of the Congo* *sadikiarsenetb@gmail.com*
Honoré Ciraba	*Department of Geodesy, Goma Volcano Observatory* *142, Avenue du Rond-Point, Quartier des Volcans, Goma City,* *Democratic Republic of the Congo* *honoreciraba@yahoo.fr*
King Iragi	*Department of Geodesy, Goma Volcano Observatory* *142, Avenue du Rond-Point, Quartier des Volcans, Goma City,* *Democratic Republic of the Congo* *honoreciraba@yahoo.fr*
Jonathan Kavuke	*Department of Geodesy, Goma Volcano Observatory* *142, Avenue du Rond-Point, Quartier des Volcans, Goma City,* *Democratic Republic of the Congo* *jkavuke@gmail.com*
Sandra Nzamu	*Department of Geodesy, Goma Volcano Observatory* *142, Avenue du Rond-Point, Quartier des Volcans, Goma City,* *Democratic Republic of the Congo* *iragiking7@gmail.com*
Bonheur Ngangu	*Department of Geodesy, Goma Volcano Observatory* *142, Avenue du Rond-Point, Quartier des Volcans, Goma City,* *Democratic Republic of the Congo* *bonheurrugain@gmail.com*
Niche Mashagiro	*Department of Technics, Goma Volcano Observatory* *142, Avenue du Rond-Point, Quartier des Volcans, Goma City,* *Democratic Republic of the Congo* *bonheurrugain@gmail.com*
Marcellin Kasereka	*Geochemistry Department,* *Goma Volcano Observatory. 142, Avenue du Rond-Point, Quartier des Volcans, Goma City, Democratic Republic of the Congo* *marcellinkasereka16@gmail.com*
Mathieu Yalire	*Geochemistry Department,* *Goma Volcano Observatory. 142, Avenue du Rond-Point, Quartier des Volcans, Goma City, Democratic Republic of the Congo* *yaliremat@yahoo.fr*
Bo Galle	*Chalmers University of Technologie,* **Hörsalsvägen 11, Floor 4** *bo.galle@chalmers.se* *http://www.chalmers.se/en/Pages/default.aspx*

Michael Poland	*U.S. Geological Survey, Cascades Volcano Observatory* *1300 SE Cardinal Court, Suite 100* *Vancouver, WA 98683* *mpoland@usgs.gov* *https://www.usgs.gov/staff-profiles/michael-poland*
Marcello Liotta	*Istituto Nazionale di Geofisica e Vulcanologia* *Via Ugo La Malfa, 153* *90146 - Palermo (Italy)* *marcello.liotta@ingv.it* *https://sites.google.com/ingv.it/marcello-liotta/*
Yosuke Aoki	*Earthquake Research Institute, University of Tokyo* *1-1 Yayoi 1, Bunkyo-ku- Tokyo* *113-0032, Japan* *yaoki@eri.u-tokyo.ac.jp* *http://www.eri.u-tokyo.ac.jp*
Adriano Nobile	*KAUST – King Abdullah University of Science and Technology* *Earth Science and Engineering - Crustal Deformation and InSAR group* *adriano.nobile@kaust.edu.sa*
Gaetana Ganci	*Istituto Nazionale di Geofisica e Vulcanologia* *Piazza Roma, 2 - 95125 Catania* *gaetana.ganci@ingv.it*
Annalisa Cappello	*Istituto Nazionale di Geofisica e Vulcanologia* *Piazza Roma, 2 - 95125 Catania* *annalisa.cappello@ingv.it*
Cristina Proietti	*Istituto Nazionale di Geofisica e Vulcanologia* *Piazza Roma, 2 - 95125 Catania* *cristina.proietti@ingv.it*
Sven Borgstrom	*Istituto Nazionale di Geofisica e Vulcanologia,* *Vesuviano Observatoy, Italia* *sven.borgstrom@ingv.it*
Mario Mattia	*Istituto Nazionale di Geofisica e Vulcanologia* *Piazza Roma, 2 - 95125 Catania-Italia* *mario.mattia@ingv.it*
Eugenio Privitera	*Istituto Nazionale di Geofisica e Vulcanologia* *Piazza Roma, 2 - 95125 Catania-Italia* *eugenio.privitera@ingv.it*
Mauro Coltelli	*Istituto Nazionale di Geofisica e Vulcanologia* *Piazza Roma, 2 - 95125 Catania* *mauro.coltelli@ingv.it*
Sebastien Valade	*Universidad Nacional Autónoma de México* *Instituto de Geofísica* *valade@igeofisica.unam.mx*
Diego Coppola	*Dipartimento di Scienze della Terra, Università degli Studi di Torino* *TORINO, Italia* *diego.coppola@unito.it*
Cristiano Tolomei	*Istituto Nazionale di Geofisica e Vulcanologia* *Osservatorio Nazionale Terremoti* *Via di Vigna Murata 605, 00143 Rome, Italy* *cristiano.tolomei@ingv.it*
Lisa Beccaro	*Istituto Nazionale di Geofisica e Vulcanologia* *Osservatorio Nazionale Terremoti* *Via di Vigna Murata 605, 00143 Rome, Italy* *lisa.beccaro@ingv.it*
Elisa Trasatti	*Istituto Nazionale di Geofisica e Vulcanologia* *Osservatorio Nazionale Terremoti*

	Via di Vigna Murata 605, 00143 Rome, Italy *elisa.trasatti@ingv.it*

Scientists/science teams issues

The involvement of local scientists in the processing and interpretation of data, both the EO and ground-based has made a step forward through their trainings abroad but there still much to improve. We shall continue with hybrid trainings of local scientists to further improve their capacity.

3. In situ data

Type of data	Data provider	How to access	Type of access
Seismic	*Goma Volcano Observatory (GVO)*	*Published papers** *Contact GVO***	*Unregistered Public*
GPS	*GVO*	*Contact GVO***	*GSNL scientists*
Gas measurements	*GVO*	*Published papers** *Contact GVO***	*Unregistered Public* *GSNL scientists*
Surface waters chemistry including Lake Kivu	*GVO*	*Published papers** *Contact GVO***	*Unregistered Public* *GSNL scientists*
Rainwater chemistry	*GVO*	*Published papers** *Contact GVO***	*Unregistered Public* *GSNL scientists*

**Published data are freely accessible; the Goma Volcano Observatory may be contacted for guidance in case of issues*

***Archived unpublished data or recently collected data are available on request, and based on the data policy for data sharing and management among the Virunga Supersite scientific community.*

In situ data issues

Some in situ data that were collected in partnership with international collaborators may still not accessible to other scientists, despite the Data Policy that was proposed by the Supersite and approved by the GVO's staff, after they have amended it (the data policy is available here, http://geo-gsnl.org/wp-content/Documents/Supersites/Virunga/History/Virunga%20Supersite_Data%20Policy.pdf). In this data policy, it is stipulated that the "ground-based data and results should be made available for full and open access after publication or in any case within 2 years ("embargo period") since their collection/generation". In any case, the GVO authorities and that of other local institutions should be contacted to get the requirements as per accessing in situ data.

4. Satellite data

<In the table below please list all satellite data types available for the Supersite>

Type of data	Data provider	How to access	Type of access
COSMO-SkyMed	*ASI*	*POC requests access from ASI for GSNL scientists individual users, data then accessible via UNAVCO*	*GSNL scientists*
Pleiades	*CNES*	*POC requests access from CNES for individual users*	*GSNL scientists*
Sentinel-1 a/b	*ESA*	*https://scihub.copernicus.eu/*	*Registered public*
ASTER ***EO-1 (Hyperion)*** ***MODIS***	*NASA*	*https://terra.nasa.gov/about/terra-instruments/modis* *https://modis.gsfc.nasa.gov/*	*Registered public*
Landsat	*USGS*	*https://www.usgs.gov/land-resources/nli/landsat/landsat-data-access?qt-science_support_page_related_con=0#qt-science_support_page_related_con*	*Registered public*
AVHRR	*NOAA*	https://earth.esa.int/web/guest/missions/3rd-party-missions/current-missions/noaa-avhrr	*Registered public*
SAOCOM 1	*CONAE*	http://saocom.asi.it:8081/#/home	*GSNL scientists*

5. Research results

5.1. In situ Data

5.1.1. Seismology : imaging the details of the crustal and the upper mantle structure along the Kivu Rift zone

1. Introduction

The Kivu rift formed in one of the highest elevation regions of the Western Rift Valley of Africa (WRA) hosts Africa's two most active volcanoes: Nyiragongo, and Nyamuragira and other dormant volcanoes and eruptive vents lie under Lake Kivu and its flanks. The Lake Kivu Basin constitutes a transition zone of the WRA from the predominant north-westerly orientation of the Rusizi–Tanganyika Rift Basin to the more southwest to the northeast trend of the Lake Kivu, Virunga, and Rutsuru–Lake Edouard Rift Basins (Ebinger, 1989a). The NE-SW faults dominate the Lake Kivu region. They belong to the Mesoproterozoic Karagwe-Ankole Belt and are overprinted, to the west of Lake Kivu, by NNE-SSW faults of the Neoproterozoic Itombwe Synclinorium which reoriented the rift direction (Villeneuve, 1987; Villeneuve and Chorowicz, 2004). This zone has experienced moderate to large earthquake (e.g The 24 October Kalehe earthquake Mw6.2; the 03 February 2008 Bukavu-Cyangugu earthquake Mw6.0; the 07 August 2015 Katana earthquake Mw5.8). These earthquakes claimed lives, more people were injured, and caused some houses to collapse (Mavonga, 2007; Mavonga, 2009; D'Oreye et al. 2011; Tuluka et al., 2020).

Studies of focal mechanisms of earthquakes occurring in the Lake Kivu region display normal faulting. Bamulezi et al., 2017 identified seismogenic faults on the Western side of the Kivu Rift associated with two distinct large seismotectonic zones. The first coincides with the northern part in which faults follow NNE-SSW orientation and the second comprises the southern part including the Rusizi river until the northern tip of the Lake Tanganyika basin with a general N–S trend, as opposed to the NE–SW trend of the Albertine-Rwenzori segment.

Earthquake hazard assessment of the Democratic Republic of Congo (DRC) Rift zone and adjacent areas including the Lake Kivu region was carried out by Mavonga and Durrheim, 2009 and Tuluka et al., 2020. Their hazard map did not take account of local geology and seismicity at a small scale due to the sparse distribution of seismic stations. Therefore, earthquakes foci were located with large uncertainty. The accuracy of earthquake location is largely dependent on the local velocity structure (Chiarabba et al., 2000).

Due to this deficiency, to fill this gap, and in order to reduce uncertainty in the location of earthquakes, we have installed additional broadband seismic stations in and around Lake Kivu with Rwanda partners. At this first stage, in the DRC side, two new seismic stations (Kalehe, KALEH; Nyabibwe, NYAB) were built and the old station (Bulengo, BULE) was repaired. These three stations

were equipped with new broadband sensors and digitizers. At the second stage, five broadband seismic stations have been or will be installed on the Rwanda side to fill the gap of coverage of seismic stations in the Lake Kivu area.

Previous study on crustal structure beneath two broadband seismic stations in the Virunga area (North of Lake Kivu, see Mavonga, 2010), determined a crust-mantle transition zone beneath the area sampled by the stations (Kunene, KNN) and (Kibumba, KBB) to be at a depth from about 30 to 41 km. In the Tanganyika rift, south of the lake Kivu region, the crustal thickness ranged from 31.6 to 39 km (Hodgson et al., 2017). Regional seismological studies reported crustal thickness estimates of 30 to 45 km in continental and global models of crustal structure (Mooney et al., 1998; Tugume et al., 2012; Laske et al., 2013). The objective of this work is to take advantage of teleseismic earthquakes waveforms recorded by seven seismic stations located in and around Lake Kivu to bring crustal P-wave velocity constraints to complement hazards studies in an area were earthquakes already damaged cities. At this first stage, seven seismological stations in D.R. Congo maintained by the "Centre de Recherche en Sciences Naturelles (CRSN)" (Lwiro, LWI and Idjwi, IDJ) and the Goma Volcano Observatory (GVO) (Goma, GOM; Bobandana, BOBN; Kalehe, KALEH; Bulengo, BULE and Nyabibwe, NYAB) were used in this study (Figure 1).
All seismic data was acquired at sample rates of 50 Hz and transmitted in real-time at Goma station base. 148 teleseismic events located between 30° and 95° from the stations shown in the figure 1 with magnitude greater or equal to 5.5 were recorded for the period from January 2016 to March 2020. We chose 80 earthquakes with a good signal-to-noise ratio which were used in the analysis. The locations of hypocenters (latitude, longitude, depth, magnitude, and region) of these teleseismic events were obtained from the USGS (Table 1). The located earthquakes and these stations are shown in Figure 2.

In this report, crustal thickness (Moho), Poisson ratio and P-wave velocities profile for seven broadband seismological stations was estimated in the Kivu Rift in the Eastern Democratic Republic of Congo using receiver function technique. P-wave receiver functions were modelled using H-k stacking analysis including error analysis through bootstrap, variance and phase weighted stacking. The first order velocity profile was obtained by inversion of receiver functions using singular-value decomposition method (SVD).

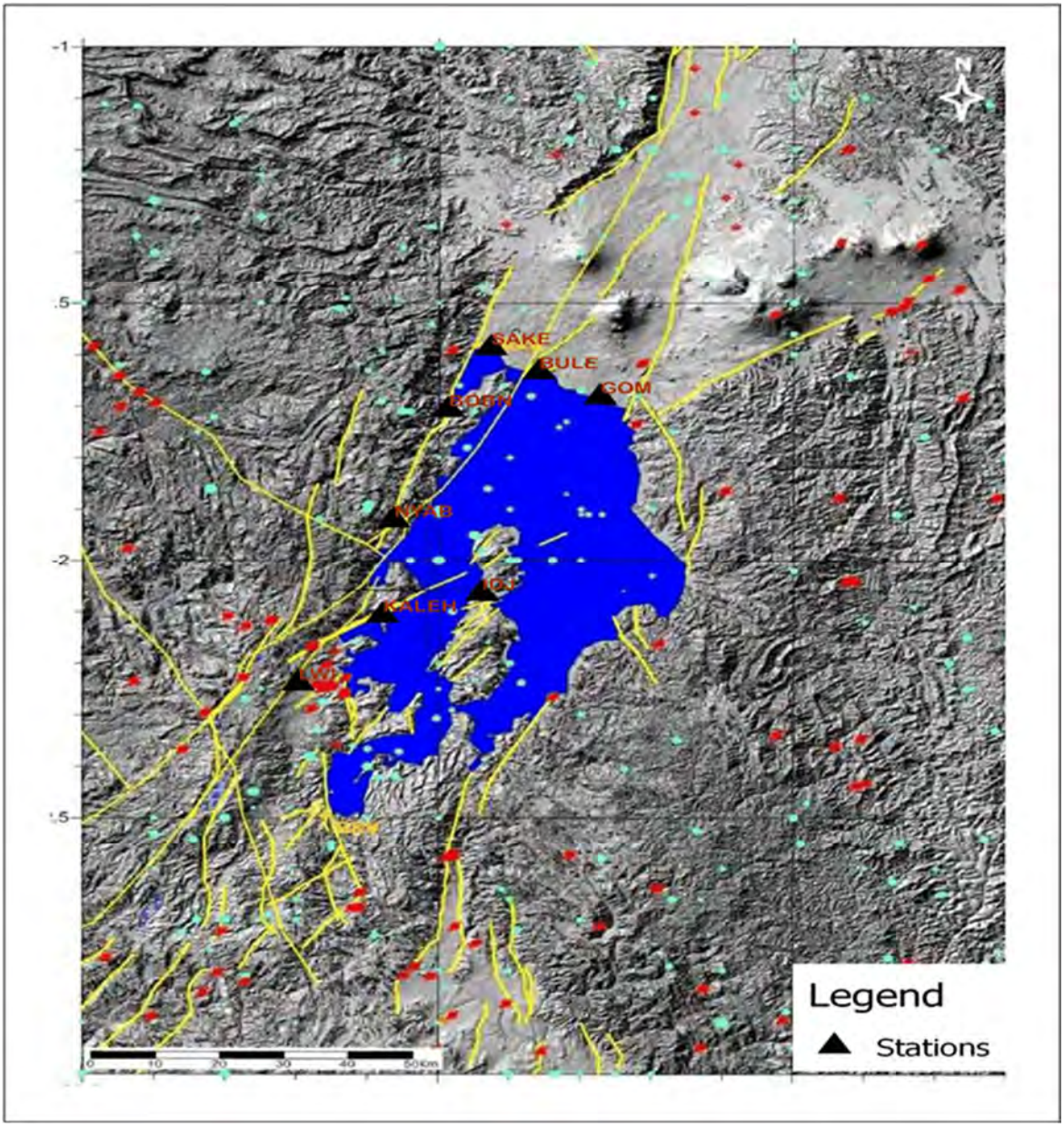

Figure 1. Seismic stations of KIVUSNet used in this work, including those acquired through the Project LKMP. These stations are represented by a black triangle.

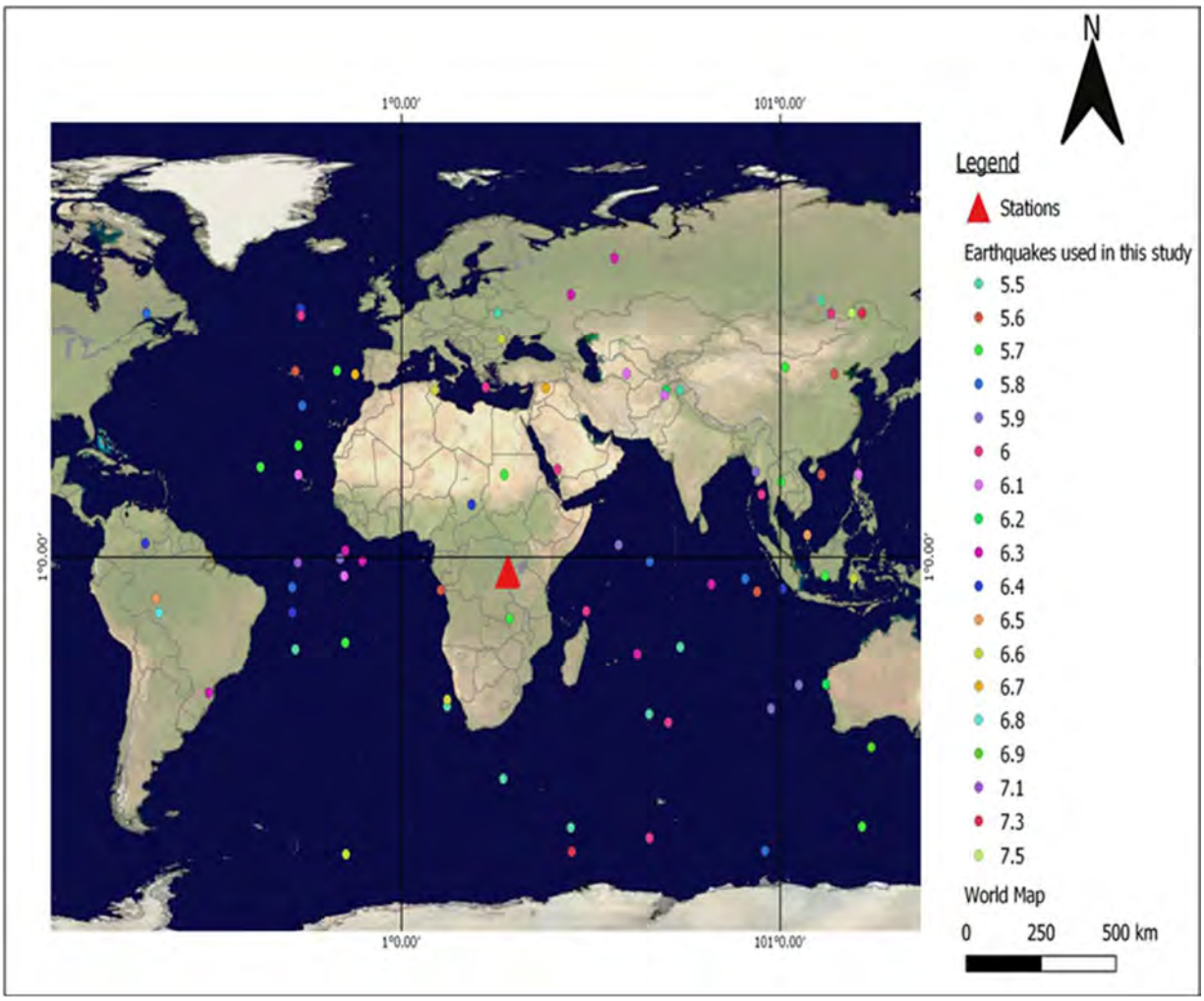

Figure 2. Distribution of earthquake epicenters used to calculate P receiver functions. The events have a magnitude larger than or equal to 5.5 with an epicentral distance between 30° and 95° from stations GOM, BLG, BOBN, NYAB, KALEH, IDJ, and LWI. These stations are represented by a triangle.

Table 1. List of Teleseismic earthquakes used in this study

Time	Latitude	Longitude	Depth		Place
2016-04-24T08:37:59.850Z	-17.9138	-27.027	10	5.5	42km SW of Bristol Island, South Sandwich Islands
2016-05-13T07:01:10.270Z	-31.3513	66.3878	10	5.5	27km WSW of Qila Abdullah, Pakistan
2016-10-26T17:10:37.210Z	-29.7716	13.0528	6	5.5	8km NNW of Norcia, Italy
2016-10-30T06:40:18.670Z	-28.4144	13.0961	8	6.6	7km N of Norcia, Italy
2017-01-10T06:13:48.140Z	51.1334	122.6171	627.17	7.3	189km SSE of Tabiauan, Philippines
2017-02-07T22:03:56.390Z	-18.8916	63.2644	29.07	6.3	22km WSW of Pasni, Pakistan
2017-02-18T12:10:17.970Z	3.8133	-66.6592	222	6.4	52km NW of San Antonio de los Cobres, Argentina
2017-02-21T14:09:04.320Z	-7.5625	-63.9047	595.98	6.5	41km E of Padilla, Bolivia
2017-03-21T23:10:25.150Z	38.4933	115.3233	111.71	5.6	1km SE of Banjar Mulung, Indonesia
2017-04-05T06:09:12.200Z	38.5429	60.4363	13	6.1	61km NNW of Torbat-e Jam, Iran

Time	Latitude	Longitude	Depth		Place
2016-04-24T08:37:59.850Z	-17.9138	-27.027	10	5.5	42km SW of Bristol Island, South Sandwich Islands
2016-05-13T07:01:10.270Z	-31.3513	66.3878	10	5.5	27km WSW of Qila Abdullah, Pakistan
2016-10-26T17:10:37.210Z	-29.7716	13.0528	6	5.5	8km NNW of Norcia, Italy
2016-10-30T06:40:18.670Z	-28.4144	13.0961	8	6.6	7km N of Norcia, Italy
2017-01-10T06:13:48.140Z	51.1334	122.6171	627.17	7.3	189km SSE of Tabiauan, Philippines
2017-02-07T22:03:56.390Z	-18.8916	63.2644	29.07	6.3	22km WSW of Pasni, Pakistan
2017-02-18T12:10:17.970Z	3.8133	-66.6592	222	6.4	52km NW of San Antonio de los Cobres, Argentina
2017-02-21T14:09:04.320Z	-7.5625	-63.9047	595.98	6.5	41km E of Padilla, Bolivia
2017-03-21T23:10:25.150Z	38.4933	115.3233	111.71	5.6	1km SE of Banjar Mulung, Indonesia
2017-04-05T06:09:12.200Z	38.5429	60.4363	13	6.1	61km NNW of Torbat-e Jam, Iran
2017-04-28T20:23:17.260Z	-38.1232	125.0658	26	6.9	31km SW of Burias, Philippines
2017-04-29T10:02:12.550Z	53.6978	111.8495	10	5.5	153km SSW of Tambakrejo, Indonesia
2017-05-03T04:47:13.380Z	-33.0788	71.4438	11	6	29km NNW of Karakenja, Tajikistan
2017-05-29T14:35:21.510Z	-3.3419	120.4313	12	6.6	28km WNW of Kasiguncu, Indonesia
2017-05-30T11:29:51.800Z	23.8442	-26.2419	76	5.7	47km NNE of Bristol Island, South Sandwich Islands
2017-07-19T12:16:23.560Z	-56.6556	66.4836	10	6	Mauritius - Reunion region
2017-07-20T22:31:11.260Z	45.6313	27.4139	7	6.6	11km ENE of Kos, Greece
2017-08-08T23:27:53.080Z	-4.584	82.8317	20	6.3	109km SSE of Dostyq, Kazakhstan
2017-08-13T03:08:10.560Z	-5.4925	101.6228	31	6.4	71km W of Bengkulu, Indonesia
2017-08-18T02:59:25.640Z	-59.9212	-13.6605	35	6.6	North of Ascension Island
2017-11-11T00:36:14.980Z	-2.8766	-14.1142	10	6.1	Ascension Island region
2017-11-12T18:18:17.180Z	-59.3923	45.9592	19	7.3	29km S of Halabjah, Iraq
2017-12-15T16:47:58.230Z	5.5171	108.1743	90	6.5	1km E of Kampungbaru, Indonesia
2018-01-07T06:47:15.780Z	-6.0817	94.9055	33	5.6	85km E of Yairipok, India
2018-01-11T06:59:30.470Z	-54.597	45.7239	10	5.5	16km ESE of Mandali, Iraq
2018-01-11T18:26:24.240Z	13.8155	96.0717	9	6	40km WSW of Pyu, Burma
2018-01-23T06:34:54.980Z	-25.3656	105.9632	48.19	5.9	29km SW of Panyaungan Timur, Indonesia
2018-01-25T01:15:58.290Z	-3.4404	91.7665	10	5.8	173km W of Mohean, India
2018-01-28T16:03:03.970Z	35.1852	9.6842	10	6.6	Southwest of Africa
2018-01-31T07:07:00.290Z	35.1565	70.8507	193.73	6.2	37km S of Jarm, Afghanistan
2018-03-10T21:45:36.340Z	0.7136	-15.2095	10	5.9	North of Ascension Island
2018-04-02T13:40:34.840Z	-10.418	-63.0058	559	6.8	11km NNE of Carandayti, Bolivia
2018-04-19T21:09:17.000Z	18.9437	42.1877	10	6	Prince Edward Islands region
2018-05-23T05:44:43.810Z	19.4193	-36.2376	10	5.7	Central Mid-Atlantic Ridge
2018-06-12T23:08:28.310Z	-30.2403	98.5876	9	5.9	83km SW of Muara Siberut, Indonesia
2018-09-01T06:13:45.040Z	35.2183	74.5586	10	5.5	Mid-Indian Ridge
2018-09-18T07:27:41.320Z	-10.0929	49.7765	10	6	Southwest Indian Ridge
2018-09-28T10:02:45.250Z	51.169	119.8462	20	7.5	70km N of Palu, Indonesia
2018-10-10T18:44:55.280Z	51.0718	114.4553	9	6	40km NNE of Cungapmimbo, Indonesia

Time	Latitude	Longitude	Depth		Place
2018-10-28T00:38:11.610Z	51.1634	26.3972	151	5.5	15km SE of Comandau, Romania
2018-10-29T06:54:21.250Z	51.1338	-66.3834	10	6.3	Drake Passage
2018-10-29T20:17:22.520Z	51.0327	-66.304	10	5.8	Drake Passage
2018-11-01T19:30:20.940Z	31.9994	-25.2059	29	5.8	131km NE of Bristol Island, South Sandwich Islands
2018-11-09T01:49:40.050Z	38.4069	-11.2431	10	6.7	120km NW of Olonkinbyen, Svalbard and Jan Mayen
2018-11-09T07:54:52.560Z	39.1651	-16.0205	10	5.7	Southern Mid-Atlantic Ridge
2018-11-11T14:03:59.560Z	-26.9878	-49.8719	10	6.3	North Atlantic Ocean
2018-11-15T20:02:22.920Z	51.9836	-25.546	15	6.4	101km E of Visokoi Island, South Georgia and the South Sandwich Islands
2018-11-23T10:51:58.580Z	39.0717	-26.9882	76	5.6	46km NNE of Visokoi Island, South Georgia and the South Sandwich Islands
2018-11-25T16:37:32.830Z	54.9009	45.7443	18	6.3	15km SW of Sarpol-e Zahab, Iran
2018-11-27T12:03:27.370Z	-16.5518	-13.8275	10	5.7	North of Ascension Island
2018-11-29T20:21:44.660Z	-59.2277	96.9976	9.87	5.8	258km SSE of Sinabang, Indonesia
2018-12-11T02:26:29.420Z	-0.1042	-26.3856	133	7.1	54km N of Bristol Island, South Sandwich Islands
2018-12-30T08:39:12.450Z	39.8353	102.349	166	5.7	89km NW of Lubuklinggau, Indonesia
2019-02-18T19:30:22.900Z	-2.8415	112.8605	23	5.7	123km S of Krajan Tambakrejo, Indonesia
2019-03-20T06:34:27.835Z	-11.6371	29.531	8	5.7	16km E of Acipayam, Turkey
2019-03-30T06:27:23.331Z	0.1168	66.5343	8	5.8	Mid-Indian Ridge
2019-04-05T16:14:16.716Z	-10.3663	-27.8522	57	6.4	94km NNW of Visokoi Island, South Georgia and the South Sandwich Islands
2019-04-12T11:45:36.591Z	-54.3946	122.6143	10	5.7	102km S of Luwuk, Indonesia
2019-04-18T05:01:06.493Z	17.949	121.6501	20	6.1	8km NE of Hualian, Taiwan
2019-04-23T20:15:50.777Z	18.4552	94.5605	14	5.9	33km NW of Along, India
2019-04-29T14:19:52.499Z	62.358	57.2283	10	6.3	Carlsberg Ridge
2019-08-05T00:40:46.024Z	-5.2046	-27.8703	10	5.8	Central Mid-Atlantic Ridge
2019-09-19T07:32:01.582Z	18.0223	111.8877	617.56	5.9	74km NNE of Blimbing , Indonesia
2019-09-19T07:32:58.793Z	17.8919	111.8968	636.41	5.6	75km NNE of Sendangmulyo, Indonesia
2019-09-26T10:59:25.648Z	17.8624	28.1502	8	5.7	18km ESE of Marmaraereglisi, Turkey
2019-10-23T16:08:14.497Z	2.3481	-13.8367	10	6.3	North of Ascension Island
2019-11-02T18:08:41.113Z	17.8675	-26.2399	8	6.1	122km NNE of Visokoi Island, South Georgia and the South Sandwich Islands
2019-11-05T20:52:01.485Z	0.231	-9.3217	10	6.3	East of the South Sandwich Islands
2019-11-20T21:03:57.835Z	16.4011	101.2534	10	5.7	23km SE of Chaloem Phra Kiat, Thailand
2019-11-26T02:54:12.872Z	11.7392	19.5256	22	6.4	15km WSW of Mamurras, Albania
2019-11-27T07:23:42.383Z	35.8087	23.2284	69	6	43km NW of Platanos, Greece
2019-12-09T17:59:47.902Z	-5.7557	11.387	10	5.6	Southwest of Africa
2019-12-20T11:39:52.874Z	34.1326	70.4555	212	6.1	49km SW of Jarm, Afghanistan
2019-12-30T17:18:59.863Z	-17.427	74.6175	30.6	5.5	35km NW of Idgah, Pakistan
2020-01-24T17:55:14.076Z	35.6024	39.0704	10	6.7	10km NNE of Doganyol, Turkey
2020-01-30T01:28:05.202Z	-44.6079	27.8845	10	5.5	72km ESE of Karpathos, Greece
2020-02-05T18:12:37.734Z	-25.2226	113.0778	592.42	6.2	108km NNE of Krajan Pangkah Kulon, Indonesia
2020-02-08T14:32:58.625Z	50.6106	-25.5526	16	6	113km SSE of Bristol Island, South Sandwich Islands
2020-03-06T10:28:42.093Z	3.4639	58.3249	10	5.9	Southwest Indian Ridge

2. Results

2.1. Crustal Thickness and V_p /V_s Ratio Estimates

Using the "hkstack" program which executes an H-k stacking of receiver functions [Zhu and Kanamori, 2000], the corresponding crustal thickness h, and V_p /V_s at these 7 stations are listed in Table 2. Figure 3 shows a sample of the H-k stacking results at GOM station, where the best-estimated H and k values are indicated by the center of the 1 σ error ellipse. It also shows the receiver functions at the corresponding station along with the predicted arrival times of Ps, multiples PpPs, and PpSs+PsPs using the best-estimated H and k values.

Table 2. Average values of Crustal Thickness H and Vp/Vs Ratio

STATIONS	MOHO DEPTH (km)	Vp/Vs
GOM	38.1 ± 2.2	1.63 ± 0.05
BULE	31.5 ± 7.1	1.22 ± 0.05
BOBN	29.3 ± 2.6	1.61 ± 0.09
KALEH	29.4 ± 3.5	1.82 ± 0.09
NYAB	28.3 ± 4.6	1.79 ± 0.16
LWI	32.5 ± 1.4	1.69 ± 0.09
IDJ	27.1 ± 2.4	1.79 ± 0.10

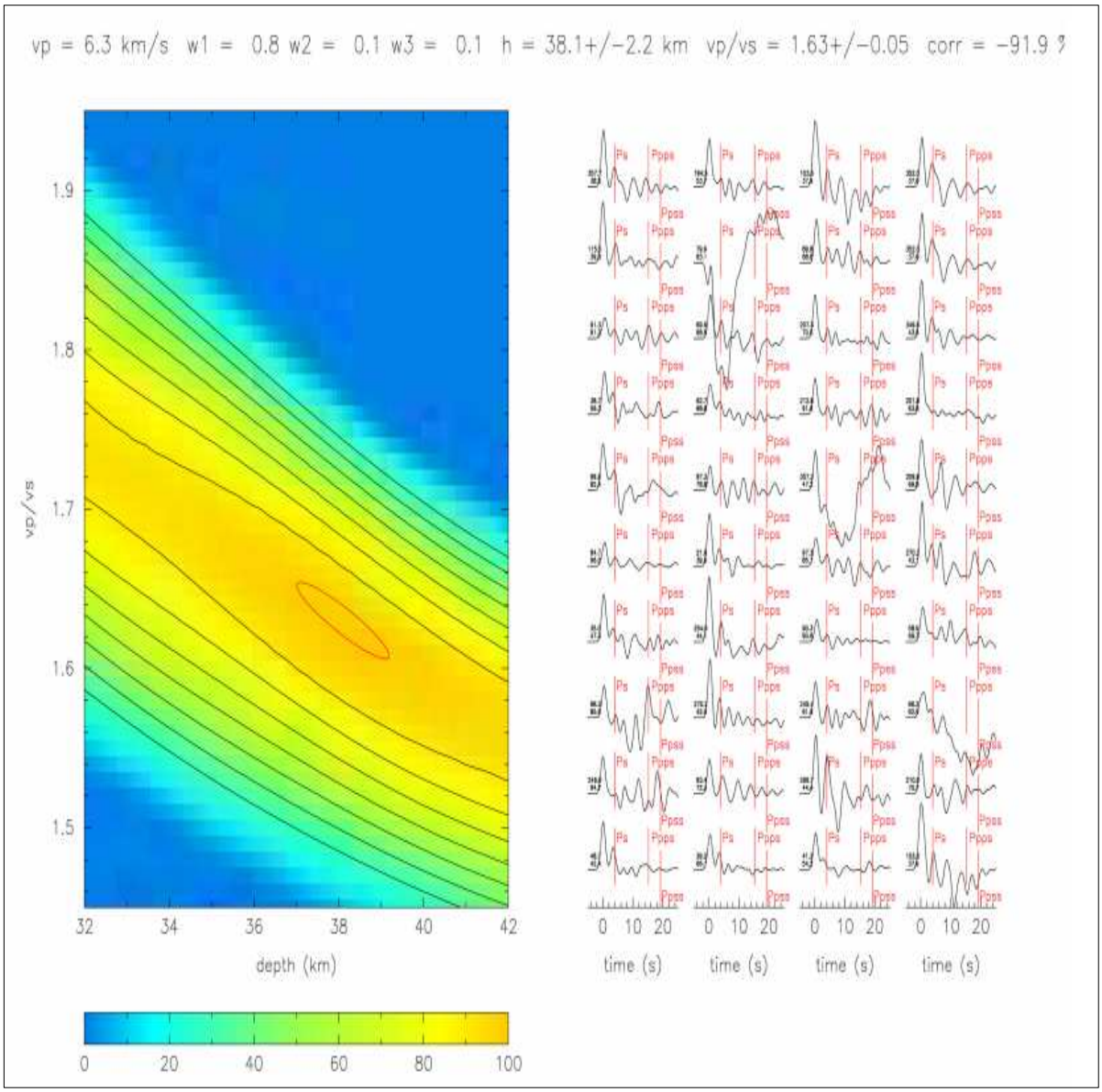

Figure 3. A sample of the H-k stacking results at station GOM where the best estimated H and k values are indicated by the center of the 1 σ error ellipse.

2.1. Inversion results of average receiver function at GOM, BULE, BOBN, KALEH, NYAB, LWI and IDJ

Using software ''manyinv" (Ammon, 1997), we achieved the final inversion models for the average receiver function obtained from G1, G2, G3, and G4 quadrants for GOM, BULE, BOBN, KALEH, NYAB, LWI and IDJ. Due to the non-uniqueness in the inversion of receiver functions, eight inversions were executed for each run with one initial model provided in Mavonga (2010). We sorted out the acceptable solutions in each inversion and selected those which fit about 80% or more of the signal power. The model produces one or more synthetic waveforms that compare well with the observed average receiver function at GOM, BULE, BOBN, KALEH, NYAB, LWI and IDJ. A sample of these synthetic waveforms at GOM, KALEH, IDJ and LWI is shown in Figure 4. The corresponding velocity

model at these last stations is shown in Figure 5. By assuming a Poisson's ratio equal to 0.25, the S-velocity model can be calculated using the relation $V_p / V_s = 1.73$. Final results are shown in Figure 6. The reduced average velocity model is listed in Table 3.

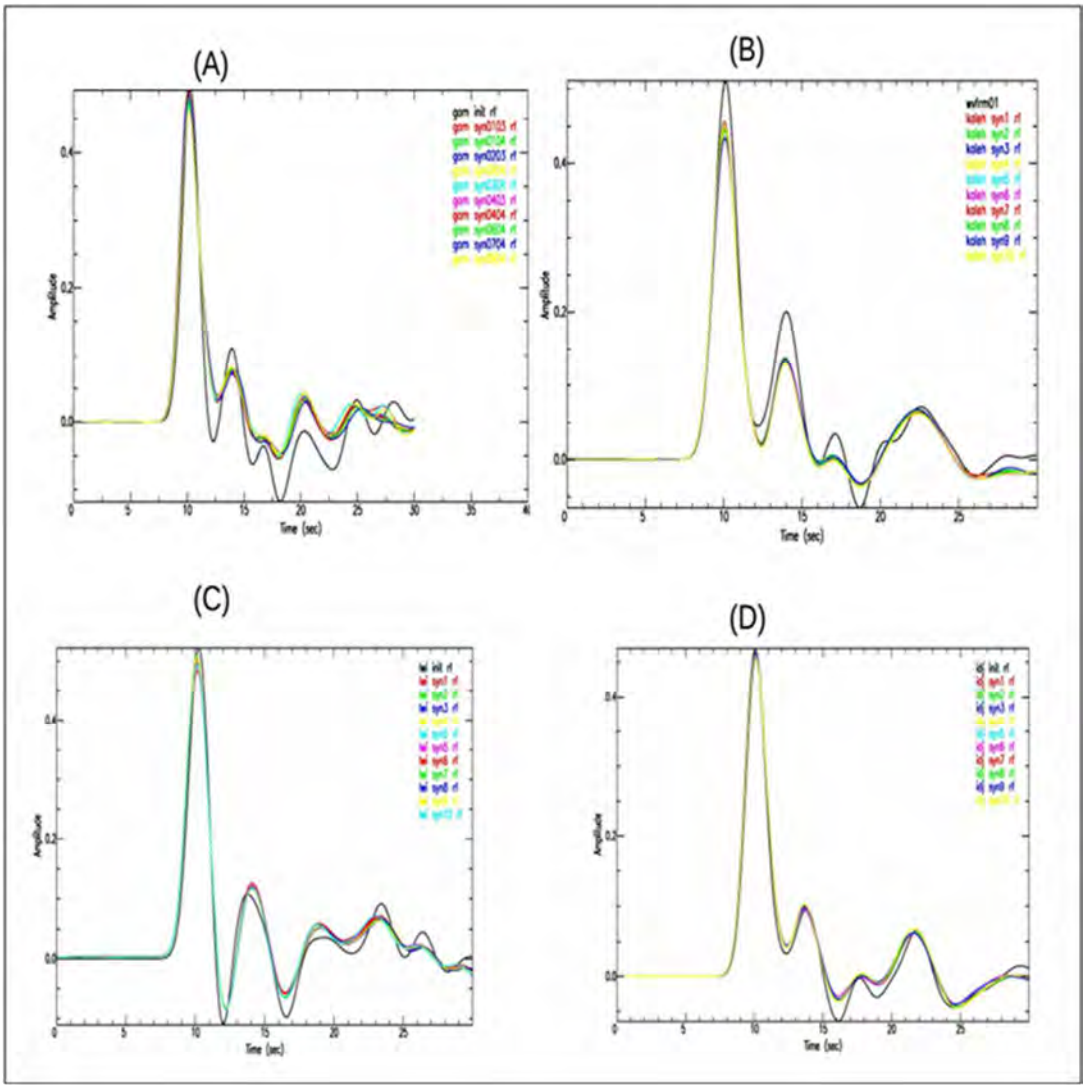

Figure 4. Synthetic waveforms that compare well with the observed average receiver function at A) GOM, B) KALEH. C) LWI, and D) IDJ. The selected waveforms fit about 80% or more of the signal power.

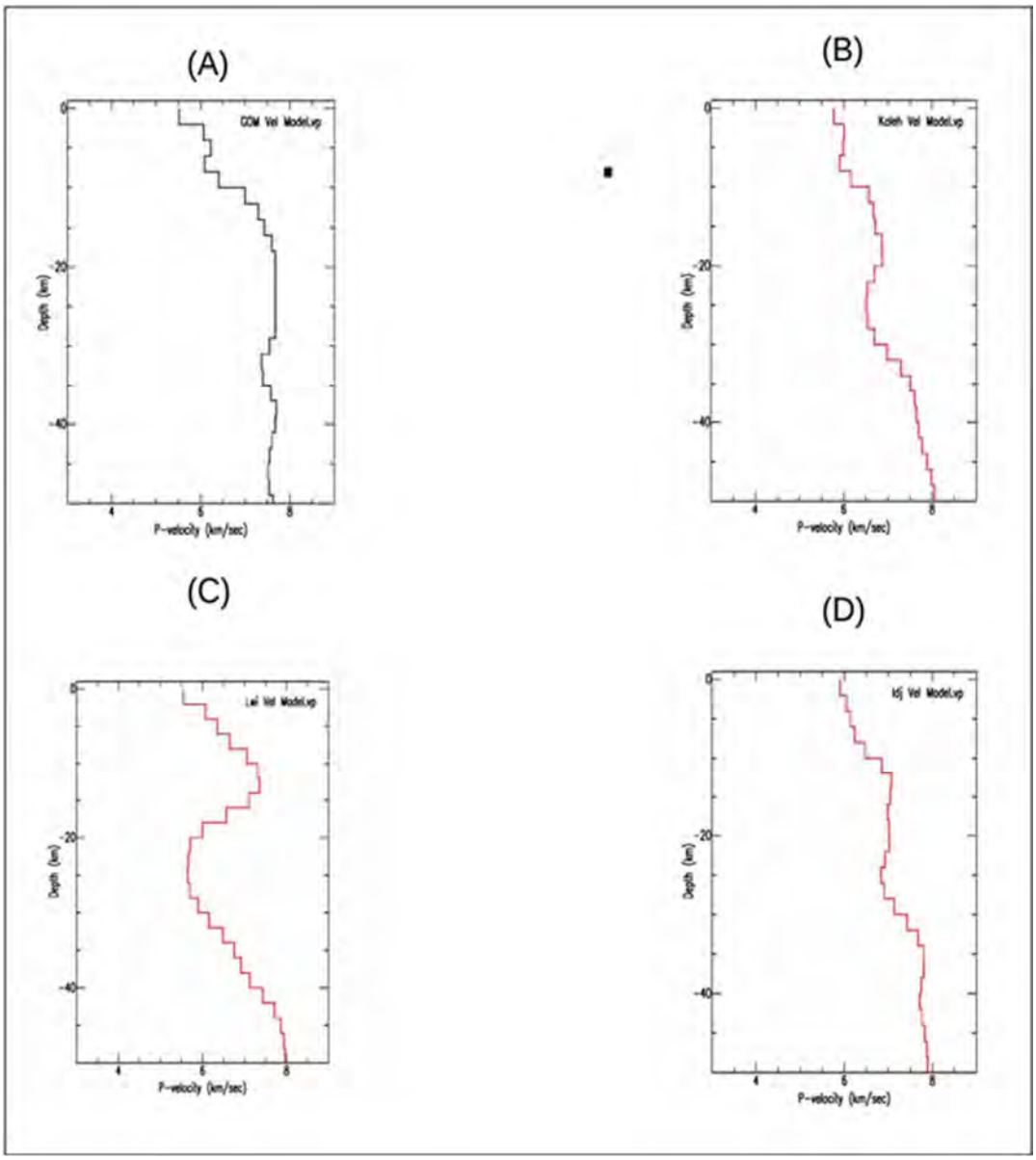

Figure 5. Velocity model obtained at each station using average receiver functions for all quadrants computed at stations (A): GOM, (B): KALEH, (C): LWI, and (D): IDJ.

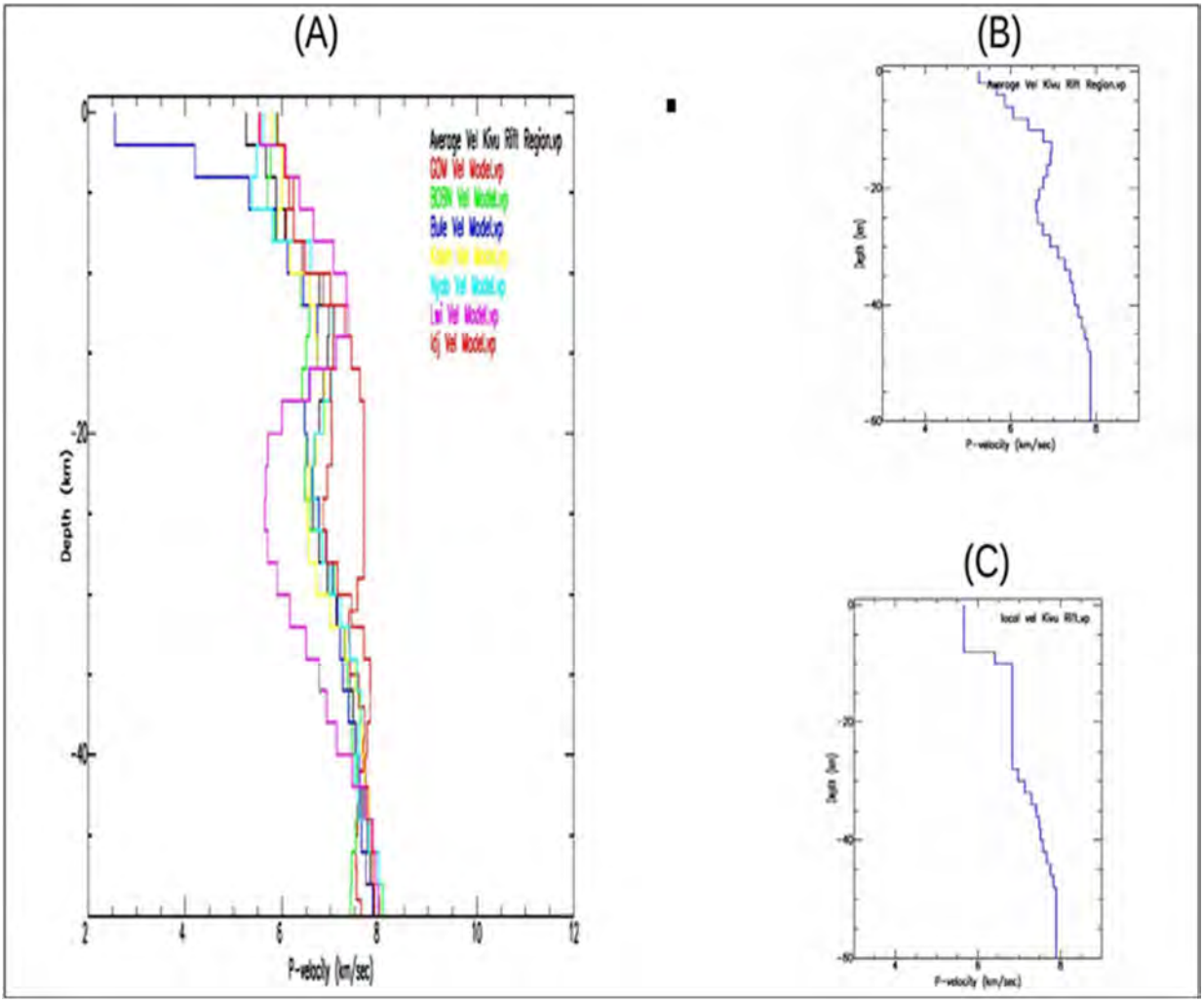

Figure 6. (A) Average velocity structure obtained by superimposing all velocity structures obtained at GOM, BULE, BOBN, KALEH, NYAB, IDJ, and LWI, respectively. (B) Kivu Region average structure simplified from the arithmetic mean of velocity at each layer in (A). (C) Simplified model created by combining layers in (B) embedded in alternating layers of high and low velocities and showed only the average velocity, taking layer thickness into account as shown in Table 3.

Table 3. Average local velocity in the Kivu Rift Region

Vitesse de l'onde P V_p(km/s)	Top of the layer (km)
5.67	0.0
6.42	8.0
6.83	10.0
6.97	28.0
7.14	30.0
7.29	32.0

7.41	34.0
7.48	36.0
7.52	38.0
7.57	40.0
7.66	42.0
7.76	44.0
7.84	46.0
7.89	48.0

3. Discussion

3.1. Crustal Thickness and V_p /V_s Ratio

From the work of Zana et al (1992) on gravity data obtained from the North of Lake Kivu Region survey, South of Virunga volcanic complex, it was observed that the negative Bouguer gravity anomalies decrease from East to West. The two-dimensional model of these anomalies indicates that a surface layer of low-density material fills a V-shaped trough structure beneath the Lake Kivu area. The Goma station, used in this study, is located on the eastern edge of the V-shaped trough. The crustal thickness beneath the Goma station varies from 36 to 40.0 km. The lower and upper bound of crustal thickness from West to East varies between 24 to 36 Km and 30 to 40 km, respectively. The crustal thickness values observed below stations BOBN, BULE, GOM, IDJ, KALEH, NYAB, and LWI are in agreement with this density model. It decreases from East to West. Compared with published laboratory data (e.g., Christensen 1975, 1996), the V_p /V_s ratio k can be related to rock types. For common rock types, V_p /V_s is particularly sensitive to composition. Increasing the silica content lowers V_p /V_s and high mafic content increases it (Kern 1982). Low V_p /V_s ratio favors the presence of felsic crust rather than significant volumes of partial melts. Based on Table 3 and considering their upper values, KALEH (V_p /V_s =173-1.98), NYAB (V_p /V_s s = 1.63-1.95), IDJ (V_p /V_s s =1.69 -1.89) and LWI (V_p /V_s =1,60 - 1.78) sample a crust between felsic and mafic while BOBN (V_p /V_s =1.52-1.70) and GOM (V_p /V_s =1.58-1.68) sample a felsic crust. This high (Vp/Vs > 1.78) may indicate crustal modification by magmatic intrusion hypothesis. Figure 7 shows the Moho piercing points of rays at a depth corresponding to the Moho depth beneath stations KALEH, BOBN, NYAB, IDJ, LWI, BULE, and GOM, respectively, as shown in Table3. The Moho piercing points were computed using IASP91 (Crotwell et al., 2001). This interpretation is supported by the position of these stations located on the Western shoulders of the Kivu sector of the Western rift where a chain of strombolian cones erupted alkaline basalts and basanite during 2-0 Ma. This alkaline volcanism was coeval with transitional silica-saturated basaltic eruptions on the rift floor and subaqueously (in

part) on the bed of Lake Kivu (Kampunzu and Lubala 2012). Observation of piercing points in Figure 7 shows that our study samples also the Virunga area including volcano Nyiragongo and Nyamulagira but there is some deficit in the Rwanda side area.

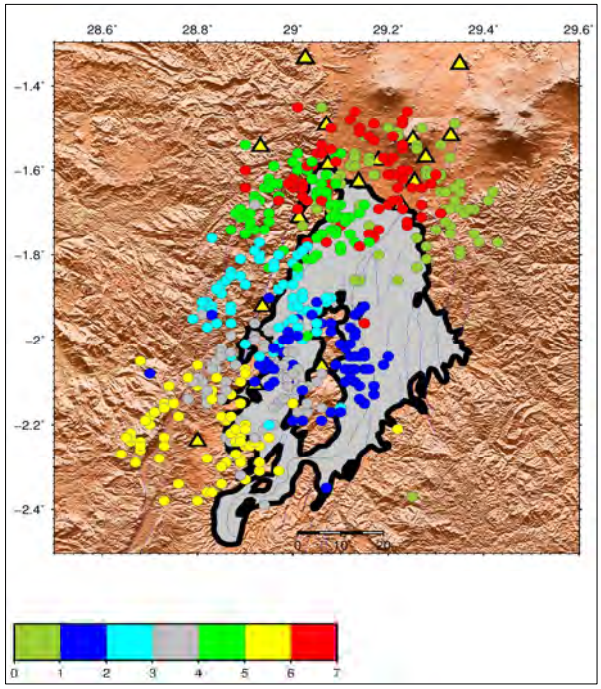

Figure 7. Moho piercing points of rays at a depth representing the Moho depth beneath stations GOM, IDJ, NYAB, KALEH, BOBN, LWI, and BULE, as shown in Table 3 and represented in the legend by colour delimited by the intervals 0 to 1, 1 to 2, 2 to 3, 3 to 4, 4 to 5, 5 to 6 and 6 to 7, respectively.

4. Conclusion and recommendations

We evaluated the structure of the crust below seismic stations KALEH, BOBN, NYAB, IDJ, LWI, BULE, and GOM by inverting stacks of teleseisms receiver functions. The resulting first order velocity models were presented as the P-wave velocity model. A lateral variation in receiver function with back azimuth was observed. This implies lateral heterogeneities or dipping of layers. The crust-mantle transition zone below the Kivu Rift region is approximative at a depth from 24 to 40 km. Based on the plot of piercing points at Moho depths, a deficit in the Rwanda side was observed. Thus, the result obtained in this study can be improved by setting up the five supplementary broadband stations at Rwanda side at Rubavu, Karongi, Waw island, Nyamasheke, and Rusizi.

References

Ammon C J (1997) Research notes & softwares. <http://eqseis.psu.edu/cammon/>

Bamulezi, G.G., Mavonga, T.G., Delvaux, D. (2017). Seismotectonic analysis of some potentially active faults on the Western side of the Kivu rift in the Democratic Republic of the Congo.Geo-Eco-Trop., 41,2, n.s.:169-186.

Christensen NI (1996) Poisson's ratio and crustal seismology. J Geophys Res 101:3139–3156, DOI:10.1029/95JB03446.

Christensen, NI and DM Fountain (1975) Constitution of the lower continental crust based on experimental studies of seismic velocities in granulite. Geol Soc Am Bull 86:227–236, DOI:10.1130/0016-7606.

Ebinger, C. J. (1989a). Geometric and kinematic development of border faults and accommodation zones, Kivu–Rusizi Rift, Africa. Tectonics, 8, 117–133.

Ebinger, C. J. (1989b) Tectonic development of the western branch of the East African rift system. Geological Society of America Bulletin 101:885–903.

Hodgson, I., IIIsley-Kemp, F., Gallacher, R.J., Keir, D., Ebinger, C.J., Mtelela, K. (2017). Crustal structure at a young continental rift: A receiver function study from the Tanganyika Rift. Tectonics, 36. https: //doi.org/10.1002/2017TC004477

Laske, G., Masters, G., Pasyamos (2013). Update on CRUST1.0 - A 1-degree Global Model of Earth's Crust. EGU General Assembly Conference Abstracts, April 2013

Mavonga, T. (2007). Some characteristics of aftershock sequences of major earthquakes from 1994 to 2002 in the Kivu Province, Western Rift Valley of Africa. Tectonophysics 439, 1–12

Mavonga, T., & Durrheim, R. J. (2009). Probabilistic seismic hazard assessment for the Democratic Republic of Congo and surrounding areas. South African Journal of Geology, 112, 329–342.

Mavonga, T., (2010). Crustal structure beneath two seismic broadband stations revealed from teleseismic P-wave receiver function analysis in the Virunga volcanic area, Western Rift Valley of Africa. Journal of African Earth Sciences, 58, 820–828

Mooney, W.D., Laske, G. and Guy Masters, T. (1998). CRUST 5.1: A global crustal model at . *Journal of Geophysical Research 103: doi: 10.1029/97JB02122. Issn: 0148-0227.*

Tugume, F., Nyblade, A., & Julià, J. (2012). Moho depths and Poisson's ratios of Precambrian crust in East Africa: Evidence for similarities in Archean and Proterozoic crustal structure. Earth and Planetary Science Letters, 355, 73–81

Tuluka, G.M., Lukindula, J. & Durrheim, R.J. (2020). Seismic Hazard Assessment of the Democratic Republic of Congo and Environs Based on the GEM–SSA Catalogue and a New Seismic Source Model. Pure Appl. Geophys. 177: 195. https://doi.org/10.1007/s00024-018-2084-6

Sadiki, A.T., Kyambikwa, A.M., Namogo, D.B. et al. Analysis of the Seismicity Recorded before the May 22, 2021 Eruption of Nyiragongo Volcano, Democratic Republic of the Congo. J. Volcanolog. Seismol. 17, 246–257 (2023). https://doi.org/10.1134/S0742046323700136

Villeneuve, M. (1978). Les centres d'emmissions volcaniques du rift africain au Sud du lac Kivu (Republique du Zaire). Revue de Géographie Physique et de Géologie Dynamique, 20, 323–334

Villeneuve, M., (1987). Géologie du synclinal de l'Itombwe (Zaïre oriental) et le problème de l'existence d'un sillon plissé Pan-africain. Journal of African Earth Sciences 6, 869-880.

Villeneuve, M., Chorowicz, J., 2004. Les sillons plissés du Burundien supérieur dans la chaîne Kibarienne d'Afrique centrale. Comptes rendus Géoscience 336, 807-814.

Zana, N., Tanaka, K., Kasahara, M., 1992. Main geophysical features related to the Virunga zone, Western rift, and their volcanological implications. Tectonophysics 209, 255–257.

Zhu L, & Kanamori H (2000) Moho depth variation in southern California from teleseismic receiver functions. J Geophys Res 105:2969–2980, DOI:10.1029/1999JB900322.

5.1.2. Measurement of sulfur dioxide in Nyiragongo volcanic plume

During an eruption, fluids often precede solids and are therefore “warning signs” of a volcanic eruption. This is why volcano observatories, including the Goma Volcano Observatory (GVO) are interested in monitoring the composition of volcanic gases, particularly of open system volcanoes.

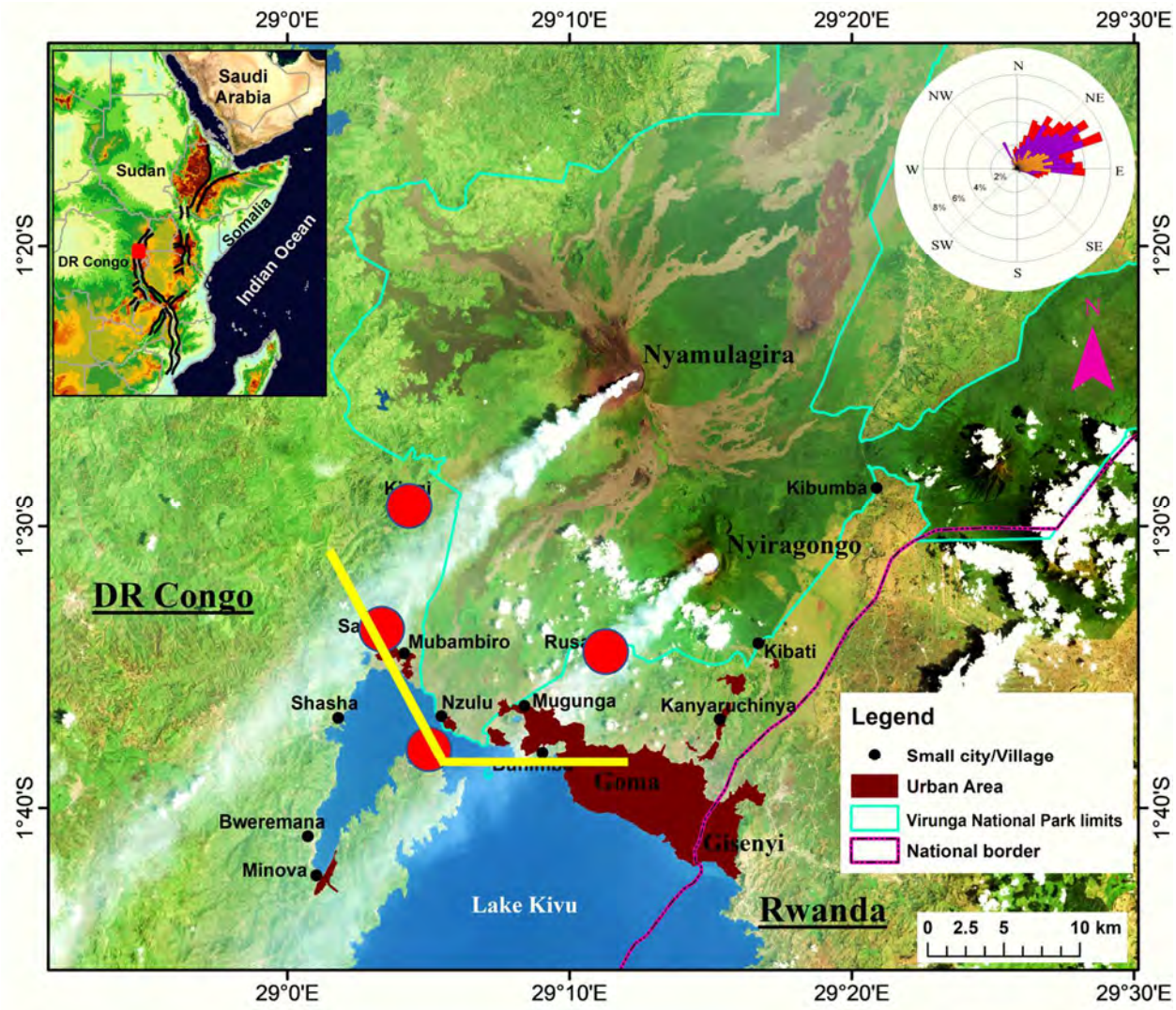

Figure 8. Map showing the location of DOAS stations sites (red dotes) around Nyiragongo and Nyamulagira volcanoes, in the north basin of Lake Kivu. The basement image shows the plumes of the two volcanoes, and image that was acquired on February 9, 2015 by the NASA’s Earth Observatory Landsat 8, accessed September 28, 2015) are shown Nyiragongo and Nyamulagira permanent plumes pushed west-southwest ward by the regional dominant wind.

Thus, the GVO studies the composition of gases from the Virunga active volcanoes, i.e. Nyamulagira and Nyiragongo, to capture any changes in their composition which would be a sign indicating possible volcanic eruption. Differential Optical Absorption Spectroscopy (DOAS) instrument is therefore used to measure sulphur dioxide (SO_2) amount in volcanic plume. Four stations were deployed around the active volcanoes with one installed in Rusayo, Sake, Kunene and another in Buzi (Figure 9). The stations experienced several technical difficulties until only the Rusayo station

operated alone before the May 22, 2021 eruption of the Nyiragongo volcano. In March 2022, two new stations were installed in Sake and Rusayo to replace those which had become dilapidated and obsolete. Currently, the network stations are therefore insufficient at the time when the technician continues to struggle for the proper functioning of Sake station. Note that only Rusayo station is functional and the data used in this report are those produced by this station. In the framework of the present study, it is planned to buy for GVO two DOAS instrument, with each consisting of a UV spectrometer, a telescope, an optical fiber, a motor-controlled scanning device, a self-contained remotely programmable microcomputer, a GPS receiver, and a timer.

- **Volume of sulphur dioxide emitted by Nyiragongo Volcano in 2023**

The collected and processed data since the beginning of 2023 come from the station installed in Rusayo, which was used to produce the below graph:

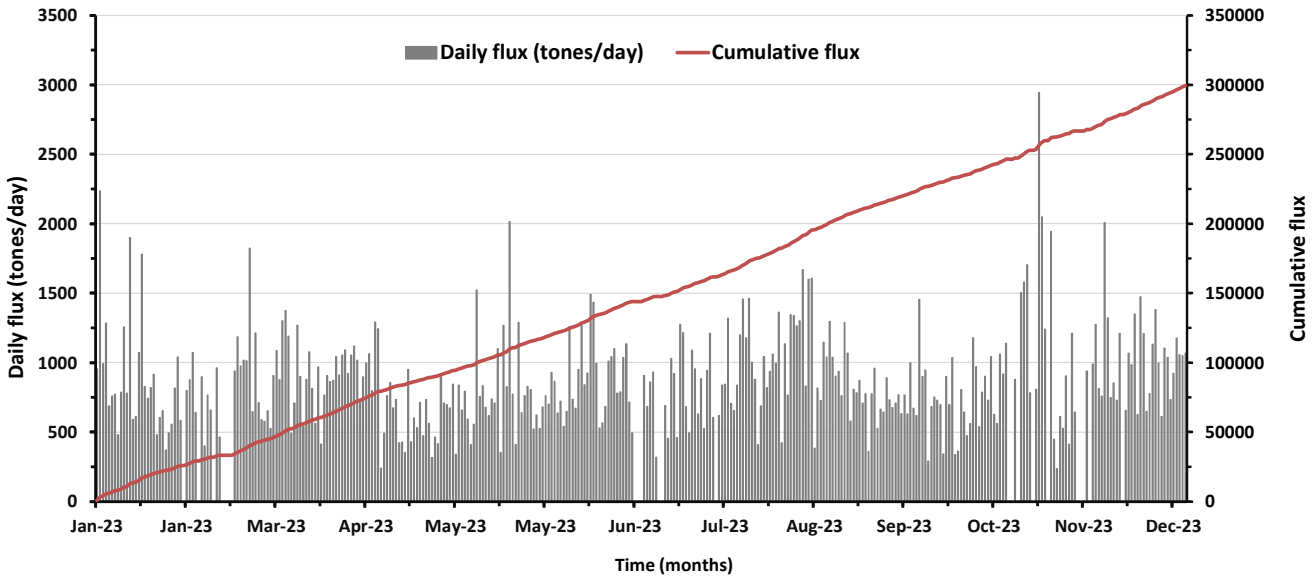

Figure 9. Chart showing the variation of SO_2 concentration in Nyiragongo volcanic plume as measured at Rusayo site between late January to December 2023 at Rusayo station shown in Figure 9.

The SO_2 flux recorded at Rusayo, along with satellite imageries (e.g. Sentinel-2 L2A), testify to a continuous effusive activity inside the crater of the Nyiragongo volcano, and which is confirmed by the visibility above the Nyiragongo crater of the gas plume during the days with good meteorological conductions and a glow of light during the night. The areas without data mostly correspond to days when the weather conditions were very bad and therefore did not allow the DOAS spectrometer to analyse the quantity of SO_2 due to the lack of sufficient sunlight. SO_2 flows vary from 235.71 tonnes/day to 2943.38 tonnes/day with an average of 872.61 tonnes/day. The vast majority of daily SO_2 flows are less than 1000 tonnes/day, which remains modest compared to the SO_2 flows already emitted by the Nyiragongo volcano during periods of high activity, in fact values of around 18,000

tonnes /day have already been recorded by DOAS at the Nyiragongo volcano. After the May 2021 eruption of the Nyiragongo volcano, activity resumed inside its crater in September 2021, and it continues to gradually increase.

5.1.3. Monitoring of Lake Kivu in the Kabuno bay

Kabuno Bay is a sub-basin of Lake Kivu located to the northwestern part of the lake (Fig. 4), limited to the north by lava flows from Nyamulagira volcano contrary to the main basin of Lake Kivu which is bordered by Nyiragongo lava flows.

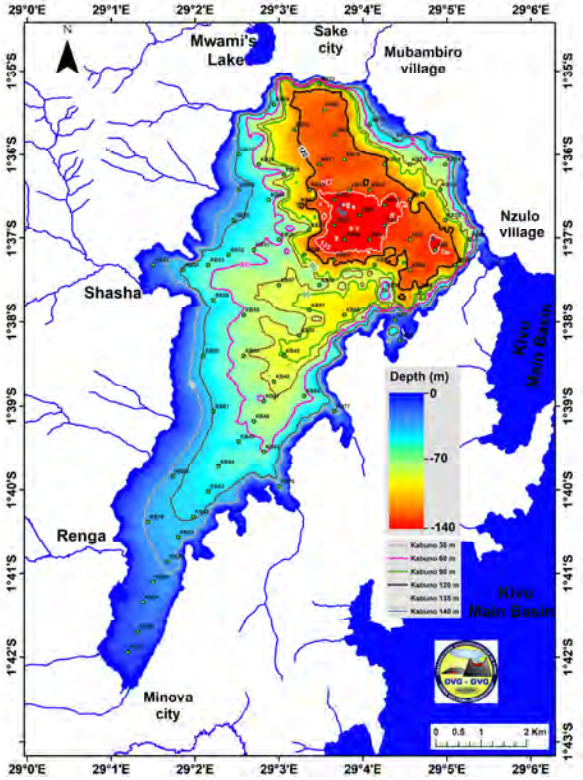

Figure 10. Map showing the sites where water samples are progressively being collected at different depth in all basins of Lake Kivu on DR Congo side except Kabuno Bay and where well as CTD profiles will be made.

This bay has a maximum depth of 140 km contrary to the Main Basin which is 485 m, but contains higher amount of carbon dioxide than corresponding depth of the Main Basin. In fact, high carbon dioxide concentration in Kabuno is found from 15 m depth, while in the Main Basin such concentration is found at about 250 m; in the Main Basin. This exposes Kabuno Bay to be more exposed to the risk of an overturn than the main basin, and conducted the RDC authorities to degassing carbon dioxide. The degassing must be done with care to not disturb the chemistry and biology of the bay, explaining the need to establishing a baseline for Kabuno Bay which consist of collecting water samples and their analysis for major cations and anions, as well as CTD multiparameter probe deployment to make vertical pH, temperature, dissolved oxygen, specific

conductivity and redox potential profiles. We also have conducted similar measurement in the main basin of Lake Kivu.

- Preliminary results show that the alkalinity of water, expressed in the form of bicarbonate, increases with depth. In the biozone or surface water (from 0 to 60m, in the main basin), the alkalinity is around 700 mg/L in the main basin (Figure 11) and around 1000 mg/L in Kabuno Bay (Figure 12). In the main basin, from a depth of 300 m to the bottom of the lake, the alkalinity is around 4500 mg/L (Figure 11), while from 40 m in Kabuno Bay the alkalinity is already at beyond 4500 mg/L and reaches values of 8500 mg/L at the bottom (Figure 12).

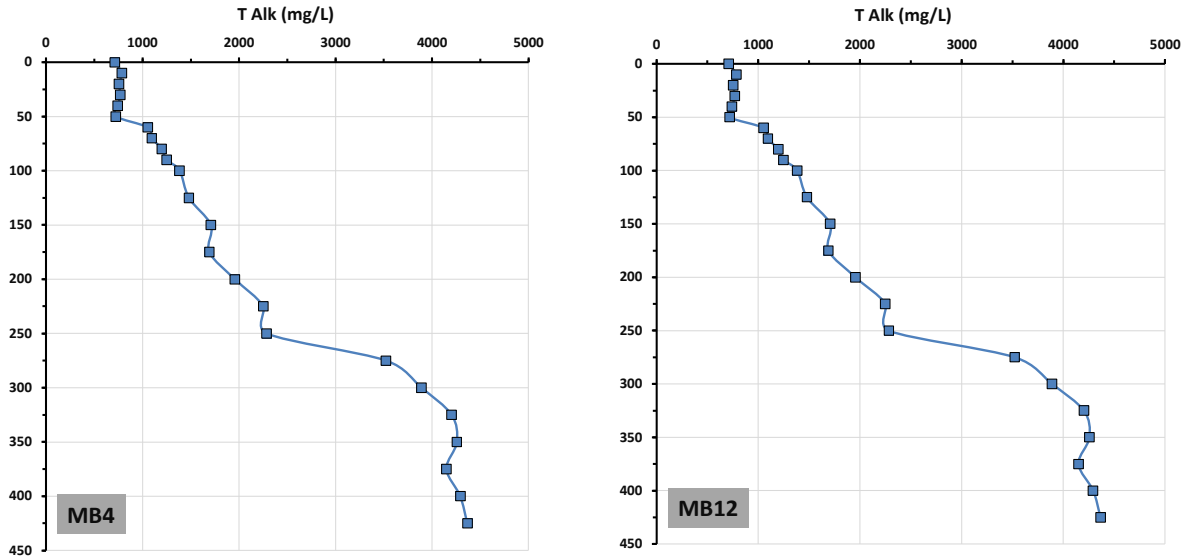

Figure 11. Vertical profiles of total alkalinity in the main basin of Lake Kivu from samples collected between January and December 2023. Total alkalinity was titrated in the form of bicarbonate (HCO_3^-) either in the field or in laboratory at the Goma Volcano Observatory (OVG), using diluted 0.1 M HCl and methyl orange as an indicator.

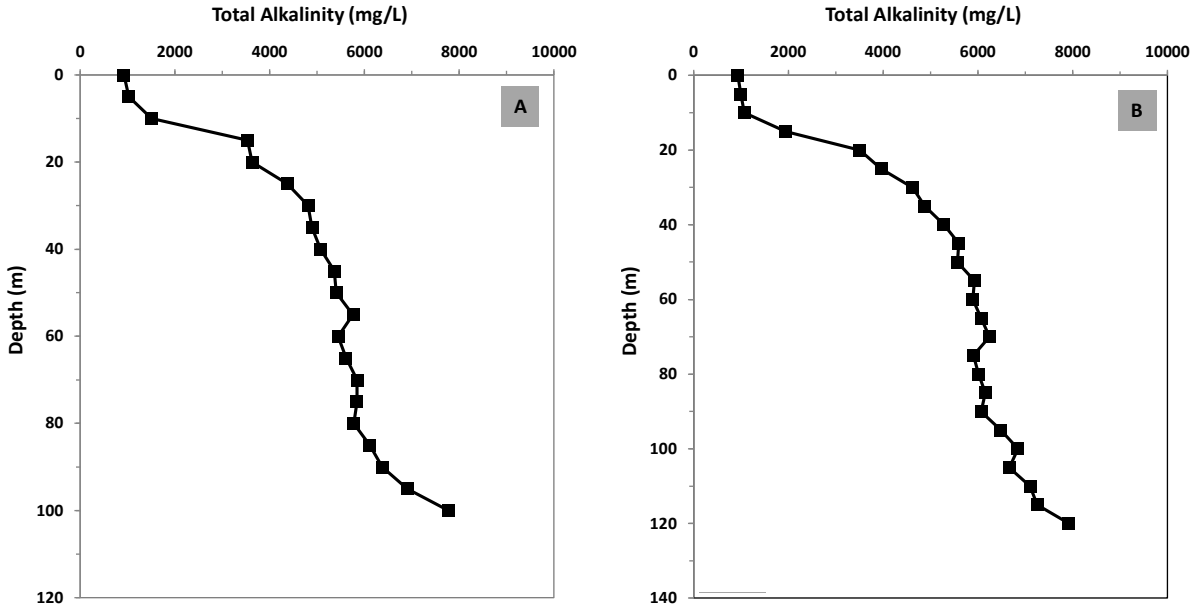

Figure 12. Vertical profiles of total alkalinity in Kabuno Bay from samples collected between January and December 2023. Total alkalinity was titrated in the form of bicarbonate (HCO_3^-) either in the field or in laboratory at the Goma Volcano Observatory (OVG), using diluted 0.1 M HCl and methyl orange as an indicator.

- The temperature profiles in the main basin (Figure 13 A) and in Kabuno Bay have the same trend (Figure 14 A), apart from the fact that in Kabuno Bay the surface waters are 1°C colder than the surface waters of the large Lake Kivu basin.

- The waters of the two northern basins of Lake Kivu have very high conductivity values and show similar increasing trends as the depth increases (Figure 13 B and Figure 14B), these high conductivities are due to the contributions from hydrothermal vents that enter the lake through underground springs and the dissolution of volcanic rocks in the northern watershed of the lake. Despite their shallow depths (140 m maximum), the waters of Kabuno Bay show very high conductivity compared to the deep waters of the large basin which is 485 m deep.

- Other parameters show similar trends. However, chlorophyll A in the surface waters of the waters of Kabuno Bay is higher than in the large basin, on the other hand, turbidity is much higher in the waters of the large basin than in those of the waters of Kabuno Bay.

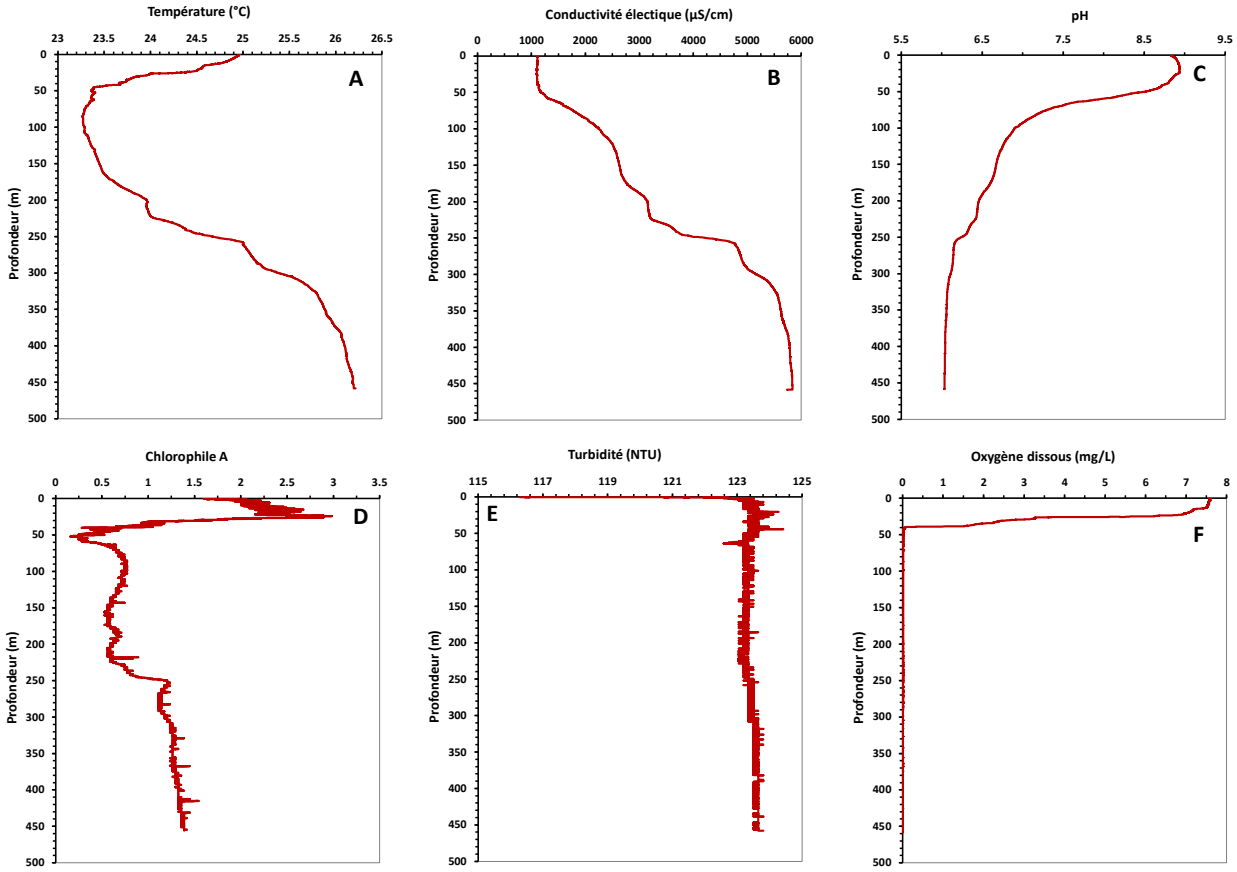

Figure 13. Vertical profiles of temperature (A), electrical conductivity (B), pH (C), chlorophyll A (D), turbidity (E), and dissolved oxygen (F) in the main basin of Lake Kivu in 2023.

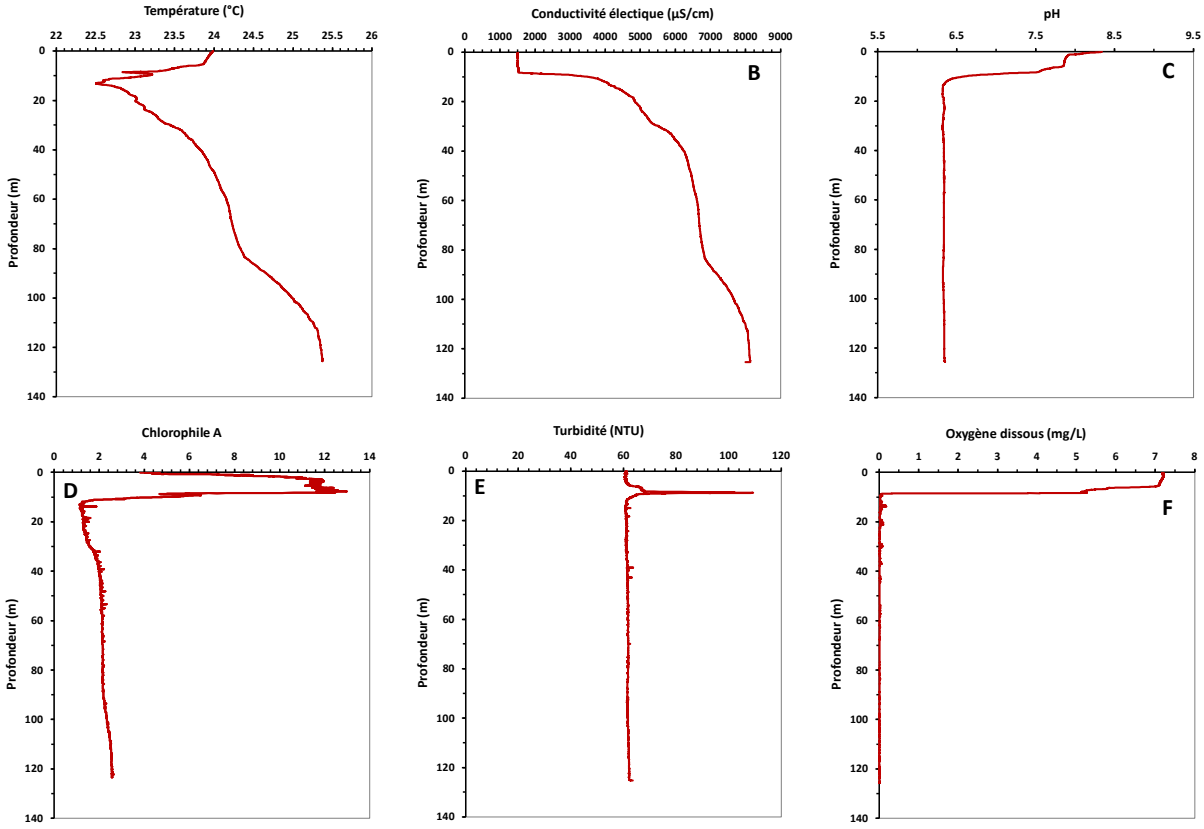

Figure 14. Vertical profiles of temperature (A), electrical conductivity (B), pH (C), chlorophyll A (D), turbidity (E), and dissolved oxygen (F) in the Kabuno bay, a sub-basin of of Lake Kivu in 2023.

References:

Cornelis Schwenk, Sophie Negele, C. Balagizi, Werner Aeschbach, Bertram Boehrer (2022) High temperature noble gas thermometry in Lake Kivu, East Africa, Science of The Total Environment, Volume 837, 2022, 155859, ISSN 0048-9697, https://doi.org/10.1016/j.scitotenv.2022.155859.

Muvundja Fabrice Amisi, Masilya Pascal Mulungula, Kisekelwa Tchalondawa Kisse, C. Balagizi, Pasche Natacha, Hyangya Béni Lwikitcha, Mudakikwa Ruhanamirindi Eric, Akonkwa Balagizi Désiré, Nahayo Déo, Ajode Z. Migeni, Stephanie Smith, Alfred Wüest, Ted Lawrence (2022) Current status and strategic way forward for long-term management of Lake Kivu (East Africa), JGLR, 2022, , ISSN 0380-1330, https://doi.org/10.1016/j.jglr.2022.04.004

Balagizi C, Marcellin M. Kasereka, Albert M. Kyambikwa, Emilio Cuoco, Ilenia Arienzo, Marcello Liotta, characterizing groundwater recharge sources using water stable isotopes in the North Basin of Lake Kivu, East Africa, Chemical Geology, 594, 2022, 120778, ISSN 0009-2541, https://doi.org/10.1016/j.chemgeo.2022.120778

Pierre-Denis Plisnier, Robert Kayanda, Sally MacIntyre, Kevin Obiero, William Okello, Anthony Vodacek, Christine Cocquyt, Hussein Abegaz, Alfred Achieng, Balagizi Akonkwa, Christian

Albrecht, C. Balagizi, et al. (2022) Need for harmonized long-term multi-lake monitoring of African Great Lakes, Journal of Great Lakes Research, 2022,ISSN 0380-1330, https://doi.org/10.1016/j.jglr.2022.01.016

Kasereka M. M., Cuoco E., Zabene Z. F., Balagizi M.C, 2021. Baseline for rainwater chemistry and quality as influenced by Nyiragongo volcano permanent plume, East Africa. Chemosphere journal. https://doi.org/10.1016/j.chemosphere.2021.130859

Balagizi and Marcello Liotta (2019). Key factors of precipitation stable isotope fractionation in Central-Eastern Africa and Central Mediterranean. Geosciences 2019, 9, 337 https://www.mdpi.com/2076-3263/9/8/337

Balagizi, Antoine Kies, Marcellin M. Kasereka, Dario Tedesco, Mathieu M. Yalire, Wendy A. McCausland (2018) Natural hazards in Goma and the surrounding villages, East African Rift System. Springer's Journal of Natural Hazards, https://doi.org/10.1007/s11069-018-3288-x

Balagizi, Marcellin M. Kasereka, Emilio Cuoco, Marcello Liotta (2018). Influence of moisture source dynamics and weather patterns on stable isotopes ratios of precipitation in Central-Eastern Africa. Science of the Total Environment Journal, 628 (629C), 1058-1078, https://doi.org/10.1016/j.scitotenv.2018.01.284

Balagizi, Marcellin M. Kasereka, Emilio Cuoco, Marcello Liotta, 2017. Rain-plume interactions at Nyiragongo and Nyamulagira volcanoes and associated rainwater hazards, East Africa, Applied Geochemistry 81 (2017) 76-89 ; http://dx.doi.org/10.1016/j.apgeochem.2017.03.018

Balagizi, Mathieu M. Yalire, Honoré M. Ciraba, Vicky B. Kajeje, Abel S. Minani, Annie B. Kinja Marcellin M. Kasereka, 2016. Soil temperature and CO_2 degassing, SO_2 fluxes and field observations before and after the February 29, 2016 new vent inside Nyiragongo crater. Bulletin of Volcanology, 78 (9):1-11, https://link.springer.com/article/10.1007/s00445-016-1055-y

Bobrowski N., Giuffrida G.B., Yalire M., Lübcke P., Arellano S., Charles M. Balagizi, Calabrese S., Galle B., Tedesco D., 2016. Multi-component gas emission measurements of the active lava lake of Nyiragongo, DR Congo. Journal of African Earth Sciences, https://www.sciencedirect.com/science/article/pii/S1464343X16302394

Coppola D., Campion R., Laiolo M., Cuoco E., Charles M. Balagizi, Ripepe M., Cigolini C., Tedesco D., 2016. Birth of a lava lake: Nyamulagira volcano 2012-2015, Bulletin of volcanology, https://link.springer.com/article/10.1007/s00445-016-1014-7

Balagizi, François Darchambeau, Mathieu M. Yalire, Steven Bouillon, and Borges V. Alberto, 2015. River geochemistry, chemical weathering, and atmospheric CO_2 consumption rates in the Virunga Volcanic Province (East Africa), Geochemistry Geophysics Geosystems, 16, 2637-2660, https://agupubs.onlinelibrary.wiley.com/doi/abs/10.1002/2015GC005999

Emilio Cuoco, Antonio Spagnuolo, Charles M. Balagizi, Stefano De Francesco, Franco Tassi, Orlando Vaselli and Dario Tedesco, 2012. Impact of volcanic emissions on rainwater chemistry: The case of Mt. Nyiragongo in the Virunga volcanic region (DRC), Journal of Geochemical Exploration, 125, 69–79, http://dx.doi.org/10.1016/j.gexplo.2012.11.008

Emilio Cuocoa, Dario Tedesco, Robert J. Poreda, Jeremy C. Williams, Stefano De Francesco, Charles M. Balagizi and Thomas H. Darrah., 2012. Impact of volcanic plume emissions on rain water chemistry during the January 2010 Nyamuragira eruptive event: Implications for essential potable water resources. Journal of Hazardous Materials, 244–245, 570–581 http://dx.doi.org/10.1016/j.jhazmat.2012.10.055

5.2. Satellite Data

5.2.1. The May 2023 Nyamulagira intra caldera Eruption: Change detection map from COSMO-SkyMed Imagery in the period April 28 to May 30

An analysis of the changes that occurred over Mount Nyamulagira during the 2023 May eruption is undertaken to detect and evaluate the lava flow evolution.

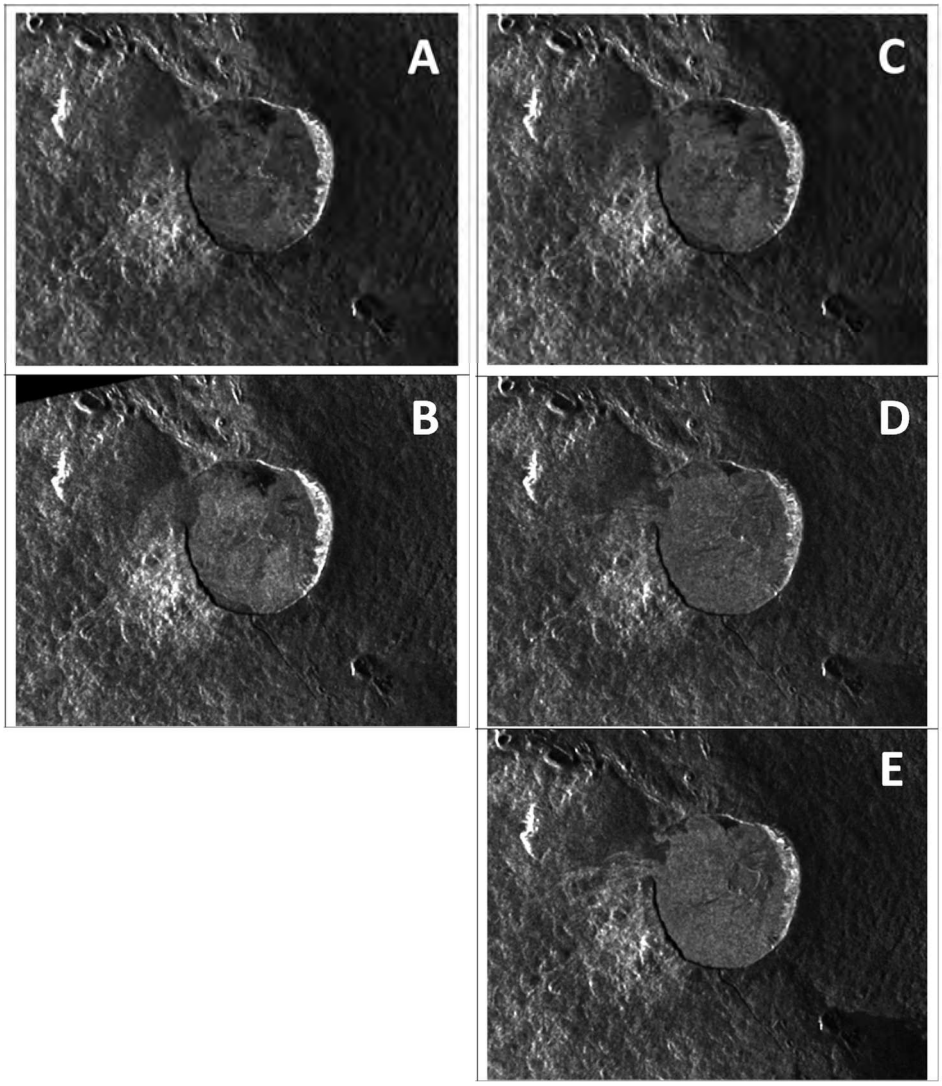

Figure 15. Results of processed CSK intensity images as for 28 April 2023, 13 May 2023, 14 May 2023, 22 May 2023, 28 May 2023

According to https://volcano.si.edu/showreport.cfm?wvar=GVP.WVAR20230517-223020, lava flows began moving into the N and NW parts of the crater beginning on 9 May, towards the low point of the crater rim. The lava continued to erupt from vents during 17-23 May.

For this analysis a time series of Synthetic Aperture Radar (SAR) COSMO-SkyMED (CSK) imagery have been used. The change detection methodology is based on the SAR intensity difference between two images collected before and after the event. Figure 15 shows the processed CSK intensity images. From the images in Figure 15, the evolution of the SAR signal intensity over the period can be appreciated in and around the Nyamulagira crater. In this case, the presence of a lava flow should be represented by a lighter shade of gray (increase of SAR signal backscattering) in the successive intensity image dates.

A visual comparison between (a) (28 April) and (b) (13 May) shows that changes inside the caldera have occurred, with a general increase of the intensity inside the crater. It can be also noted a movement of the lava flow into the NW part of the crater.

No changes are appreciated between 13 May (b) and 14 May (c).

Instead, large differences are visible between 14 May (c) and 22 May (d) due to the eruption onset. In particular, the lava flow covered the N and SW parts of the crater and it started to flow out in the W flank. In particular, the extent of the new lava coverage towards the N can be appreciated by the reduction in size of the dark area adjacent to the N rim.

The visual comparison between (d) (22 May) and (e) (30 May) shows that the lava flow continues to flow out in the W flank that, even in this case, can be appreciated by a reduction of the dark area close to the W flank.

To better identify these changes, a change detection approach based on the intensity difference is applied to each pair of contiguous CSK images. Results are shown in Figure 15 that confirms the visual intensity analysis previously undertaken. The changes associated with the lava flow are represented by dark pixels. The flank lava flow extension is manually traced and shown as a red polygon.

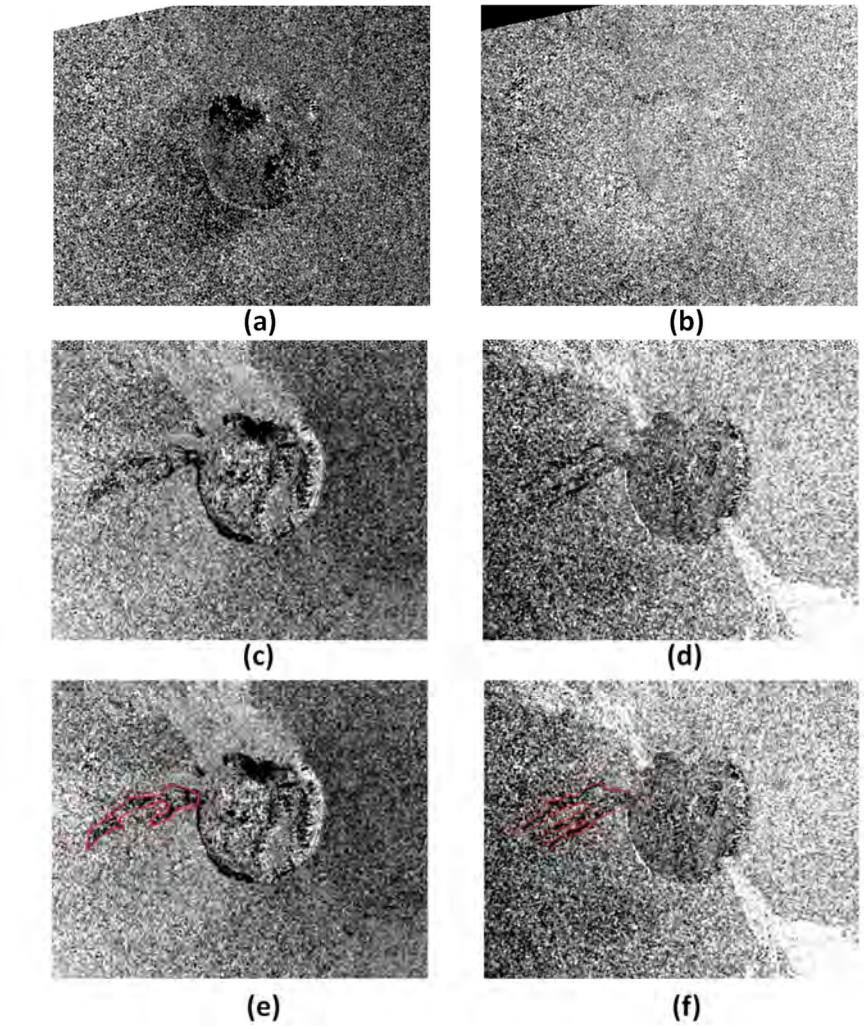

Figure 16. Change detection maps between a) 28 April and 13 May; b) 13 May and 14 May; and c) 14 May; 22 May; and d) 30 May. The changes associated with the lava flow are represented by dark pixels. The W flank lava flow pattern is evident in c) (22 May) and d) (30 May) and shown by a red polygon in e) and f), respectively.

5.2.2. The October-November 2023 Nyamulagira intra caldera Eruption monitored by satellite-based techniques

a. Change Detection mapping from COSMO-SkyMed imagery intensity signals

This section reports the analysis of the changes that occurred on Mount Nyamuragira during the 2023 October-November eruption, undertaken to detect and evaluate the lava flow evolution.

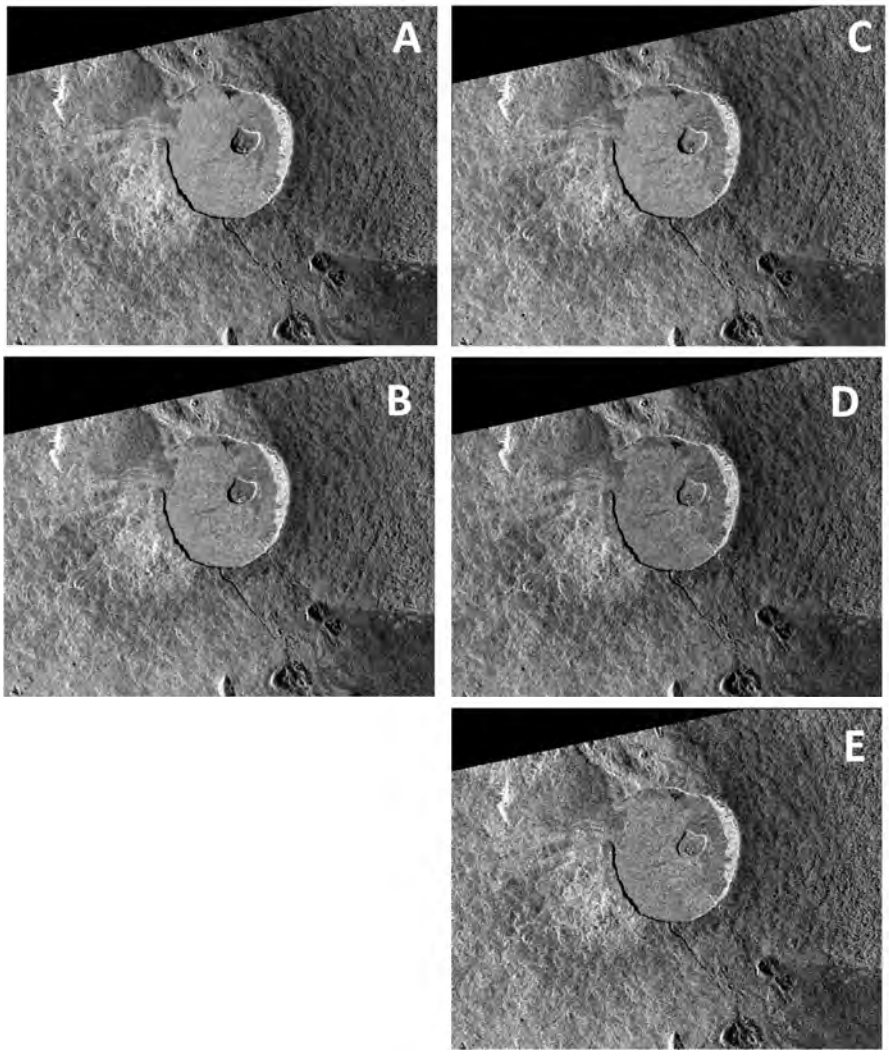

Figure 17. Processed SAR-CSG intensity images collected in ascending pass between October and November 2023, as for 3 October 2023 (A), 19 October 2023 (B), 4 November 2023 (C), 12 November 2023 (D), 12 November 2023 (E).

For this analysis, a time series of Synthetic Aperture Radar (SAR) COSMO-SkyMed Second Generation (CSG) imagery (Italian Space Agency) collected in ascending and descending passes have been used. The change detection methodology is based on the SAR intensity difference between two images collected before and after the event.

1) Ascending pass analysis

Figure 17 shows the processed CSG intensity images collected in ascending pass. The images in Figure 17 show that the SAR signal intensity evolution over the period can be appreciated inside the Nyamuragira crater. The presence of a lava flow is represented by a lighter shade of gray (because of an increase of SAR signal backscattering) in the successive intensity image dates. In particular:

- the visual comparison between (a) (3 October) and (b) (19 October) shows that changes inside the crater can be appreciated with an increase in the backscattering in (b). The two images appear similar outside the crater.
- The visual comparison between (b) (19 October) and (c) (4 November) shows changes inside the crater while no changes are visible outside the crater. However, it is worth noting that the backscattering signal decreases in (c), confirming that the lava is moving inside the crater.
- The visual comparison between (c) (4 November) and (d) (12 November) shows that even in this case, most of the changes can be appreciated inside the crater with an increase of the backscattering signal in (d).
- The visual comparison between (d) (12 November) and (e) (20 November) shows slight changes inside the crater.

To better identify the changes, a change detection approach based on the intensity difference is applied to the pair of CSG images. Results are shown in Figures 17A, B, C and D for the couple (a)-(b), (b)-(c), (c)-(d), and (d)-(e), respectively, which confirms the visual intensity analysis commented above. Most of the changes are visible inside the crater. In Figures 18A and 18C (Figures 18B and D) we can appreciate an increase (decrease) in the backscattering that is represented by a darker (lighter) area.

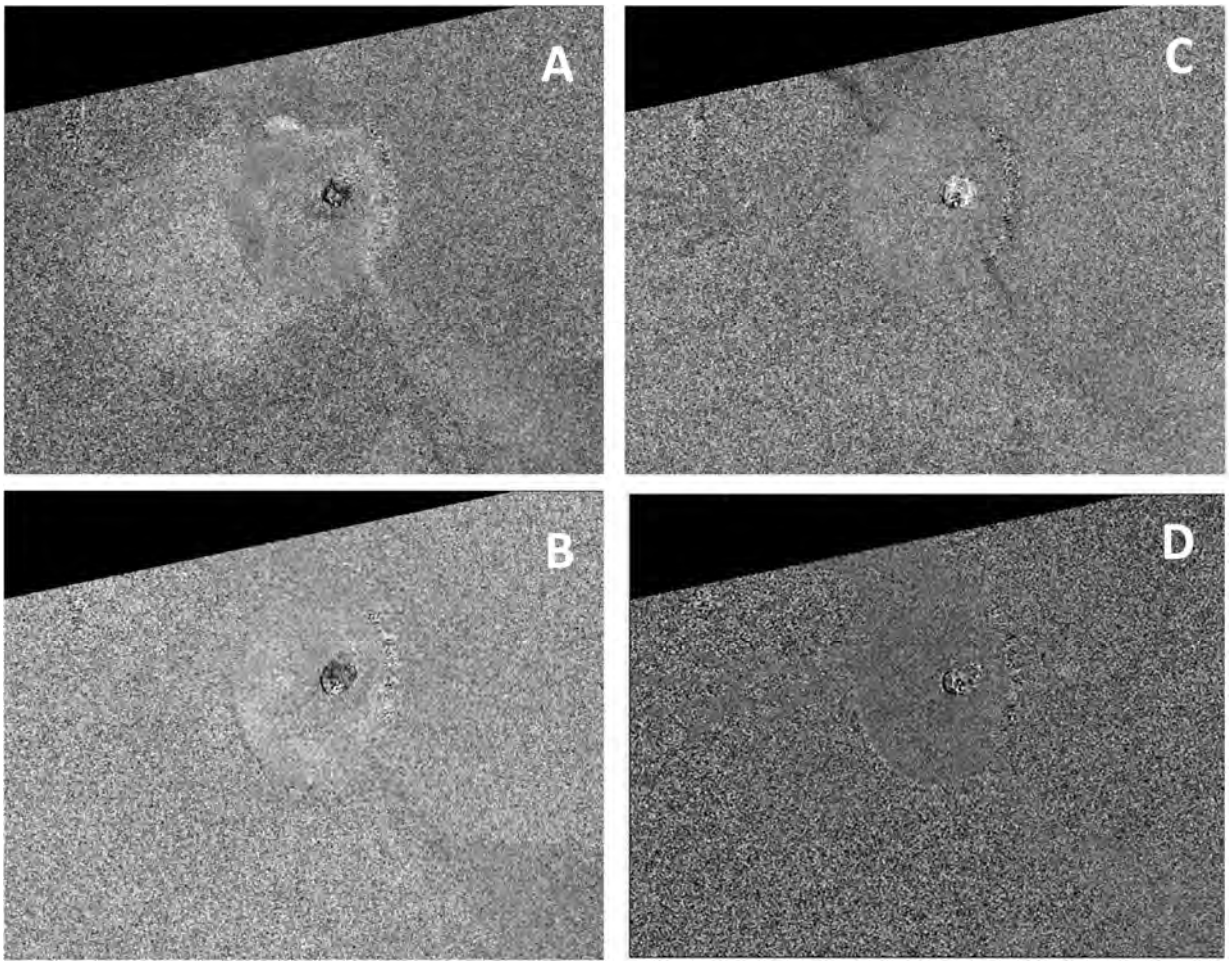

Figure 18. Change detection map between 3 October and 19 October 2023 (A), Change detection map between 19 October and 4 November 2023 (B), Change detection map between 4 and 12 November 2023 (C), Change detection map between 12 and 20 November 2023 (D).

2) Descending pass analysis

Figure 19 shows the processed CSG intensity images collected in descending pass.

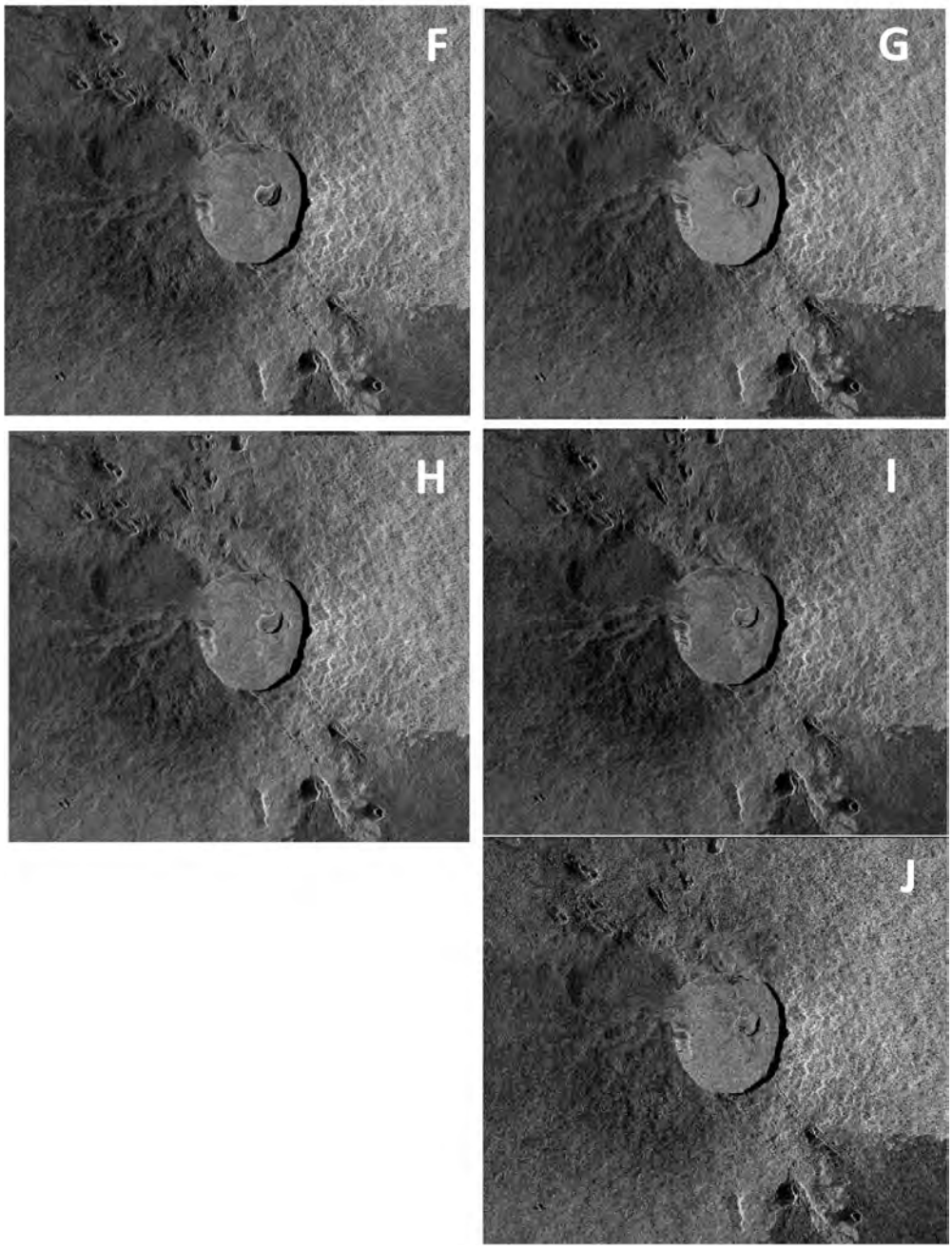

Figure 19. Processed SAR-CSG intensity images collected in descending pass between October and November 2023, for 1 October 2023 (F), 17 October 2023 (G), 2 November 2023 (H), 10 November 2023 (I), 18 November 2023 (J).

Considering the images reported in Figure 19:

- The visual comparison between (f) (1 October) and (g) (17 October) shows that changes inside the crater can be appreciated with an increase in the backscattering in (g). The two images appear similar outside the crater.
- The visual comparison between (g) (17 October) and (h) (2 November) shows changes inside the crater, while no significant changes are visible outside the crater. The backscattering signal decreases in (h), confirming that, even in this case, the lava is moving inside the crater.

- The visual comparison between (h) (2 November) and (i) (10 November) shows slight changes inside the crater with an increase in the backscattering signal in (i).
- The visual comparison between (i) (10 November) and (j) (19 November) shows no changes.

To better identify any changes, the change detection results are shown in Figures 5, 6, 7, and 8 for the couple (f)-(g), (g)-(h), (h)-(i), and (i)-(j) (of Figure 19), respectively, which confirms the visual intensity analysis discussed above. Most of the significant changes take place inside the crater. In Figure 5 (Figure 6) we can appreciate an increase (decrease) in the backscattering that is represented by a darker (lighter) area. In Figures 7 and 8, slight changes inside the crater can be appreciated

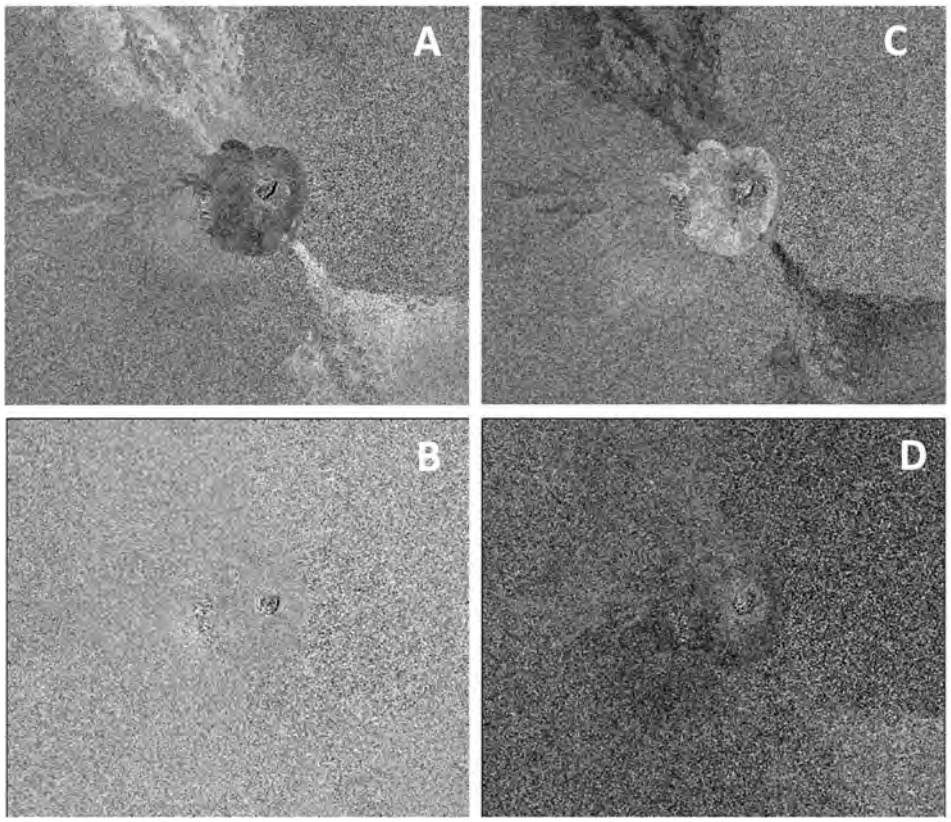

Figure 20. Change detection map between 1 and 17 October 2023 (A), between 17 October and 2 November 2023 (B), between 2 and 10 November 2023 (C), between 10 and 18 November 2023 (D).

b. Lava flow mapping from Sentinel-1 imagery coherence signals

This section reports the analysis performed with SAR images to evaluate lava flow due to the 2023 Mount Nyamuragira volcanic activity. Such analysis consists of the monitoring of the interferometric coherence variations induced by the changes due to the presence of lava. The coherence, indeed, indicates the correlation between two SAR images being sensitive to any changes of the scenario occurring in the time interval between the acquisitions. Then, any changes of the observed scenario

due to the volcanic activity produce variations of the coherence values. It can be expressed as follows:

$$\gamma = \frac{|\sum_i x_i y_i^*|}{\sqrt{\sum_i x_i x_i^* \sum_i y_i y_i^*}}$$

where *xi* and *yi* are the pixels of the first and the second SAR image.

For such analysis several pairs of SAR images acquired by Sentinel-1 missions of the European Space Agency from March to November 2023 have been used (Table 4).

Table 4. Sentinel-1 SAR dataset used for the coherence variations analysis.

Date 1	**Date 2**
March 18th, 2023	April 11st, 2023
May 5th, 2023	May 17th, 2023
May 17th, 2023	May 29th, 2023
June 10th, 2023	June 22nd, 2023
October 20th, 2023	November 1st, 2023
November 1st, 2023	November 13th, 2023

Figure 21 shows coherence maps estimated from Sentinel-1 SAR images.

a) March 18th - April 11st

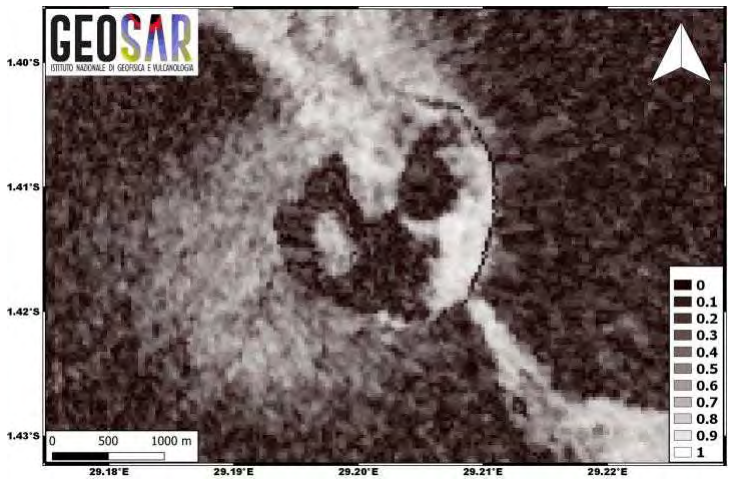

b) May 5th - May 17th	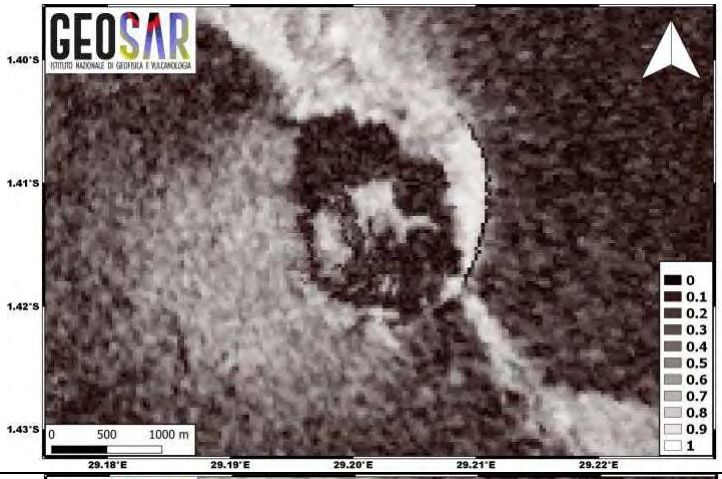
c) May 17th - May 29th	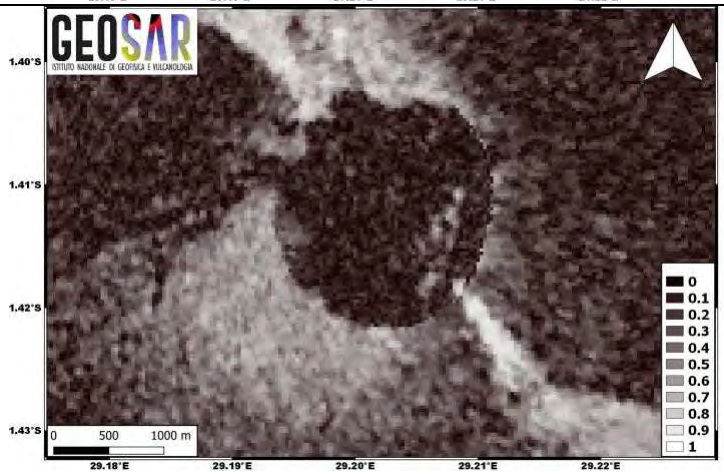
d) June 10th - June 22nd	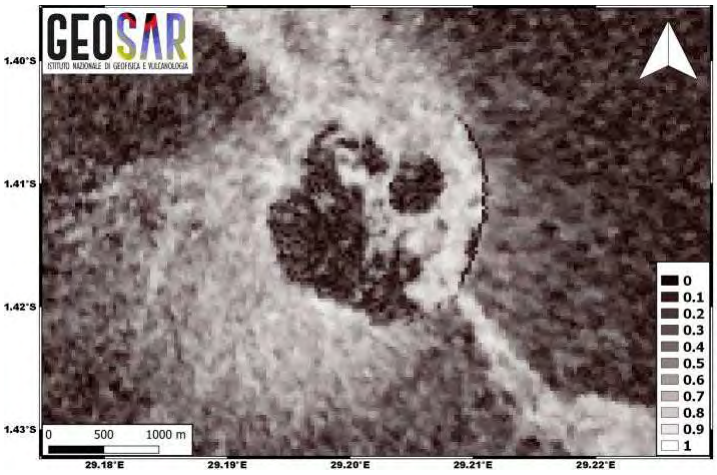

e) October 20th - November 1st	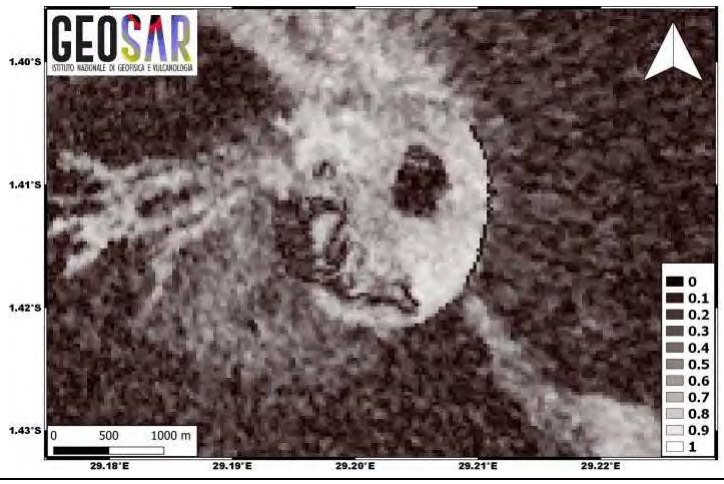
f) November 1st - November 13th	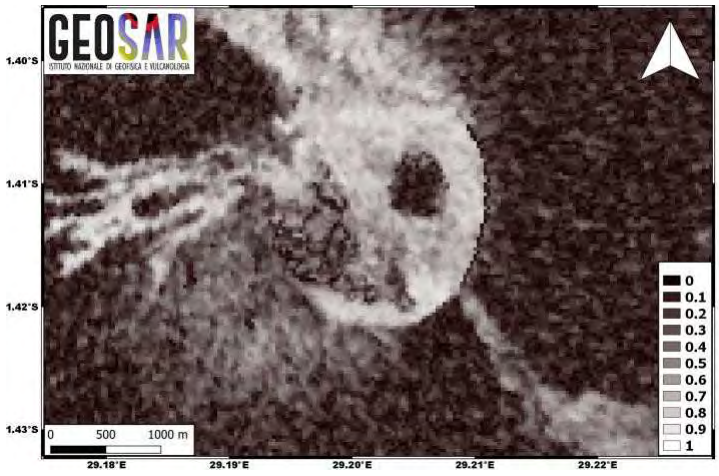

Figure 21. Coherence maps estimated from Sentinel-1 SAR images.

The areas characterized by low values of coherence (black zones in Figure 21) in all the pairs outside the crater represent the areas covered by vegetation which is strongly affected by temporal decorrelation effects. Instead, the low coherence largely observed inside the crater until June is due to the presence of a lava lake characterized by lava movements and the coherence loss in the pair May 17th - May 29th corresponds to a lava flow outside the crater and on the West flank of the volcano.

No significant changes are observed in October and November. The lava field detected in May (and some other previous lava flows) is characterized by high values of coherence in the images of October and November, meaning that the lava cooled, since there are no changes between different pairs.

c. Ground deformation analysis

Thanks to the support provided by the Argentina Space Agency (CONAE) to the Virunga Supersite, it was possible to obtain two images from the SAOCOM satellite, acquired by a SAR sensor in the L band.

We investigated the ground deformation at Nyamuragira by processing the SAOCOM image pair 20231013-20231106, along the ascending orbit (incidence angle of the sensor equal to 36.24°) and in the STRIPMAP acquisition mode, calculating the interferogram shown in Figure 22.

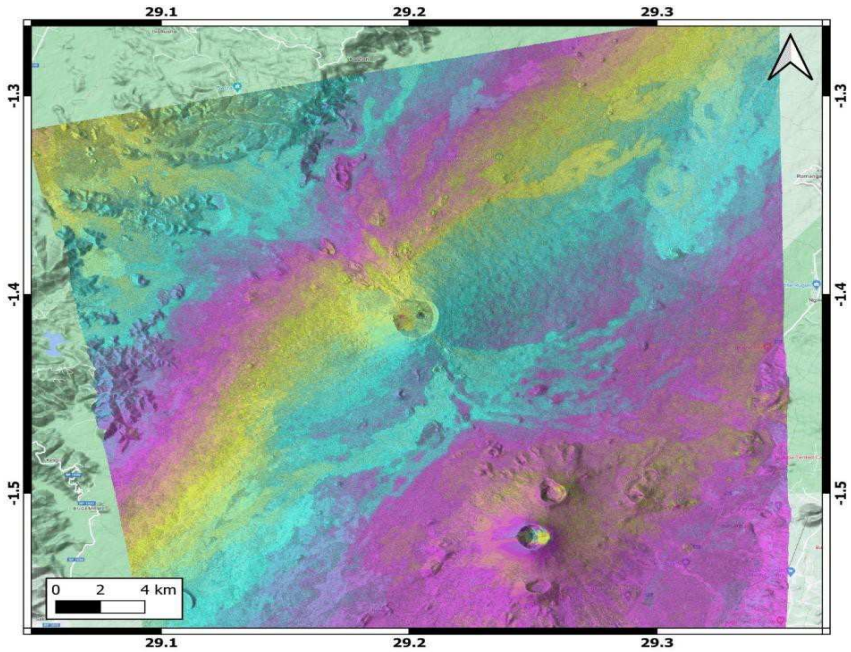

Figure 22. Wrapped interferogram from SAOCOM ascending data between October 13 and November 6, 2023.

The obtained interferogram unfortunately shows some orbital residual fringes, preventing the observation of possible ground displacement related to the unrest episode. With the aim to retrieve information about the current volcanic episode, we considered the coherence map reported in Figure 23.

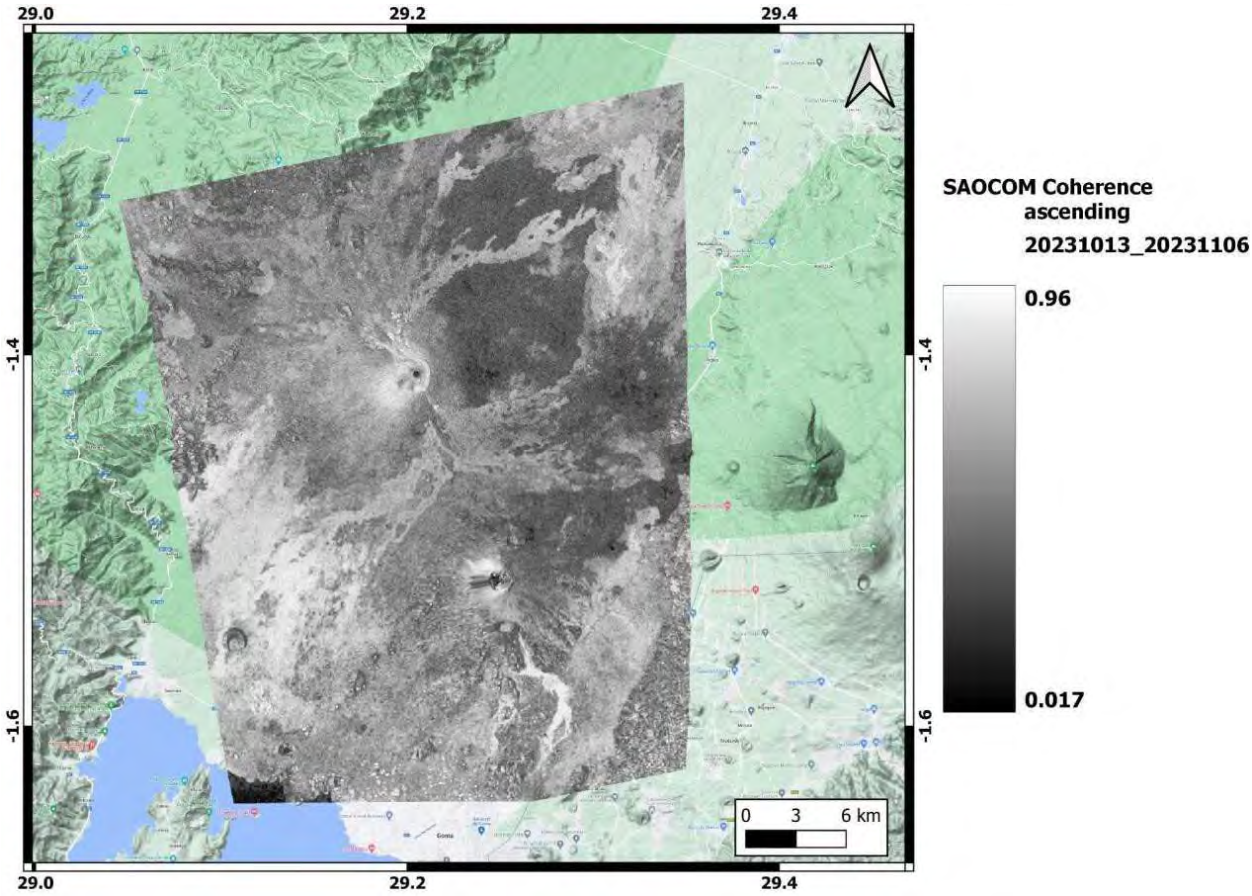

Figure 23. Interferometric coherence from SAOCOM ascending data between October 13 and November 6, 2023.

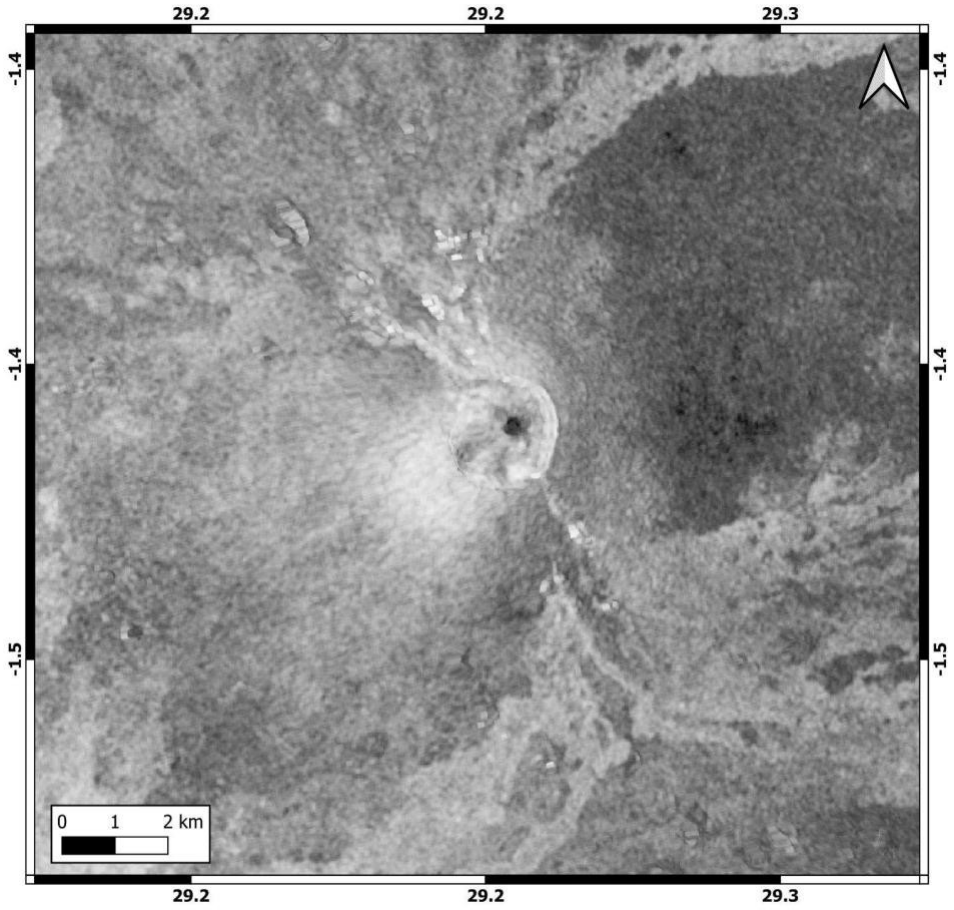

Figure 24. Zoom over the area of the Nyamuragira volcano - Coherence map.

The small black circle within the crater in Figure 11 identifies coherence loss between the two SAOCOM acquisitions (13 October and 6 November). This can be interpreted as a change of the surface that could be related to lava flow inside the crater. This result agrees with the outcomes from the coherence analysis shown previously in this report.

d. Multispectral satellite analysis

The tasking of Skysat and Prisma satellites was activated over Nyamuragira from 10 November 2023. While the Prisma satellite didn't provide good acquisitions for bad weather forecasts, the Skysat constellation, which consists of about 20 satellites, was able to acquire two scenes on 14 and 19 November (Figure 25). From these images (0.5 m spatial resolution at ground), it is possible to observe the melt portion of the lava lake extending in the south-west part of the crater and covering an area of about $15x10^3$ m^2 (insets of Figure 25).

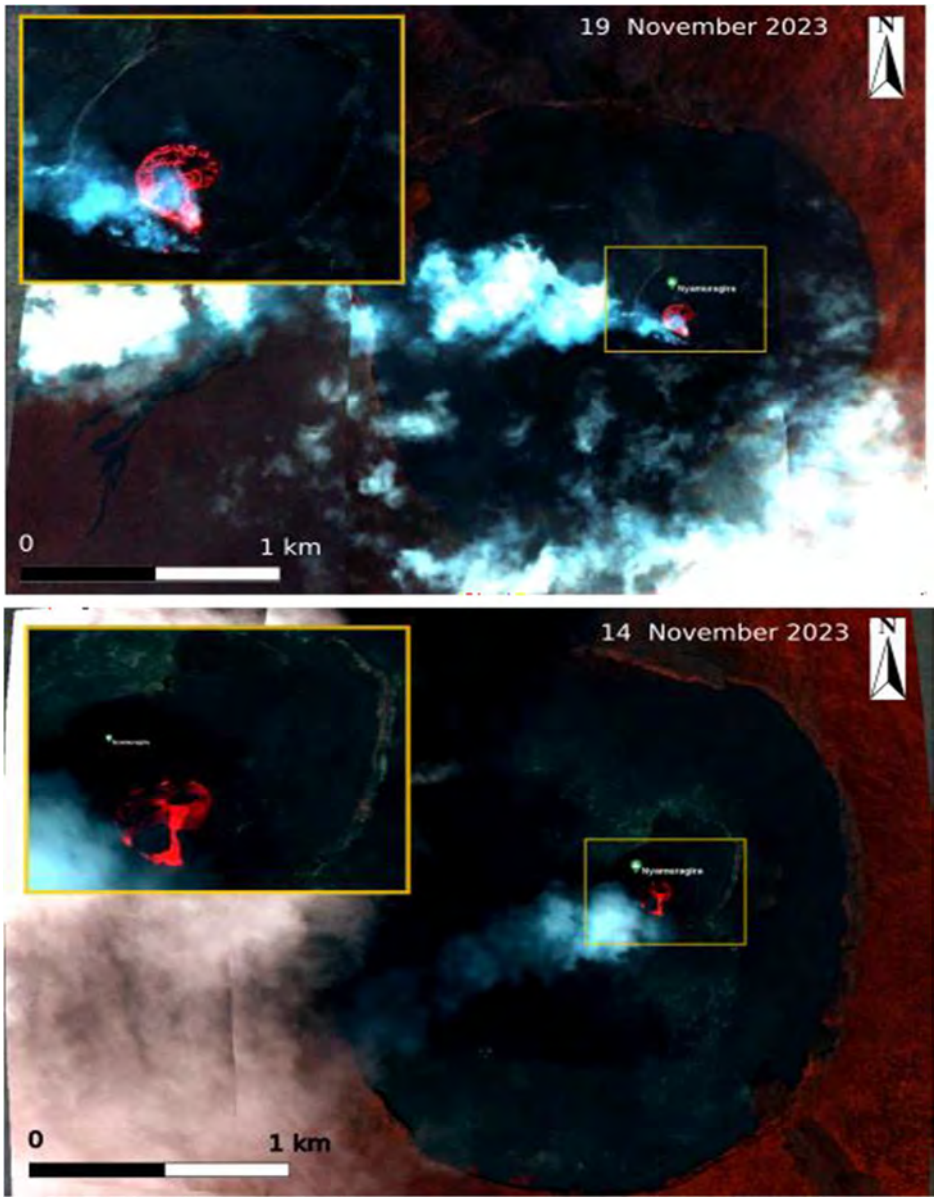

Figure 25. Skysat scenes in false-color RGB (Band 4,2,1) acquired on 19 November (top) and 14 November 2023 (bottom). Insets show the lava lake area.

By comparing the PlanetScope images (3 m spatial resolution) of 7 April 2023 and 22 July 2023, we derive the overflow occurred in May - June 2023. The lava flow outside the caldera measures about 0.9×10^6 m^2 with the longest branch reaching 3.4 km (Figure 13).

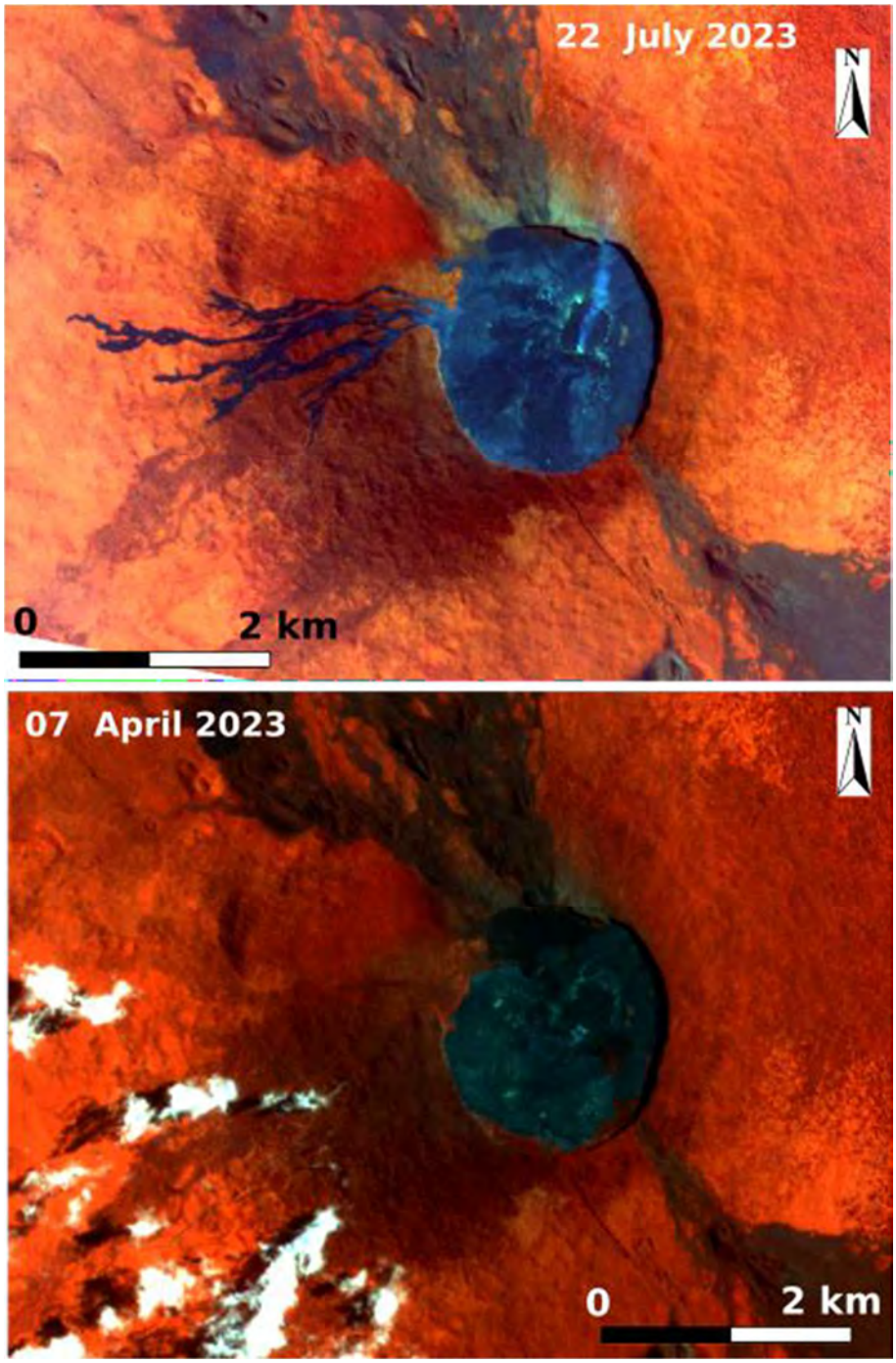

Figure 26. PlanetScope scenes in false-color RGB (Band 8,4,2) acquired on 22 July (top) and 7 April 2023 (bottom). On the top image the lava flow emplaced in May - June 2023 is clearly visible to the West of the crater.

e. Conclusions

The change detection analysis from the intensity of the SAR images (COSMO-SkyMed) in both orbits evidenced an increase or decrease of lava flow inside the crater from the beginning of

October to the end of November 2023. These changes are limited to inside the crater of Nyamuragira. The coherence mapping of the SAR images (Sentinel-1) in both orbits doesn't evidence changes inside nor outside the crater between the end of October and November 2023. On the other side, during May - June 2023 the presence of a lava lake inside the crater and coherence loss due to a lava flow outside the crater on the West flank of the volcano was detected. The interferogram from SAR images (SAOCOM) between October 13 and November 6 2023 didn't show a clear deformation pattern, although the interferogram is affected by orbital residual fringes. The interferometric coherence loss in a circle within the crater can be due to lava flow inside the crater, probably related to the June 2023 eruption as obtained through the analysis of the Sentinel-1 data. Finally, multispectral satellite imagery allowed to detect and quantify the lava flow field emplaced outside the caldera in May - June 2023 and showed how the thermal activity is currently confined in the southwest portion of the lava lake.

5.2.3. Thermal satellite monitoring of Nyamuragira volcano

The thermal activity of the Nyamuragira lava lake was followed using the CL-HOTSAT system (Ganci et al., 2016), through the processing of MSG-SEVIRI and Landsat imagery. In particular, SEVIRI data were exploited to retrieve the radiant heat flux time series, while thermal maps derived from Landsat were used to track the thermal activity.

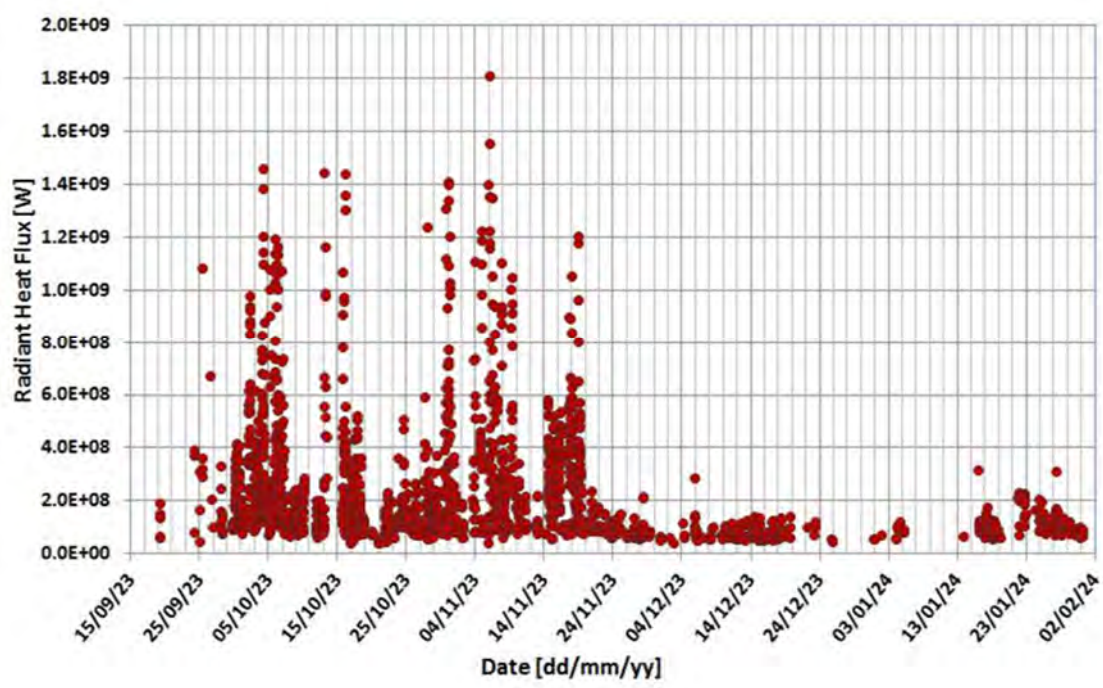

Figure 27. SEVIRI-derived radiant heat flux time series (in Watt) over Nyamuragira volcano from 15 September 2023 to 1 February 2024

The most intense thermal activity occurred from 3 October to 18 November, with peaks overcoming 1.4 GW on 4, 13, 16 and 31 October and the maximum peak of 1.81 GW reached on 5 November. After that, a clear decrease in the radiant heat flux is observed, with values mostly below 0.2 GW until 1 February. The decrease in radiant heat flux since the end of November, as well as the thermal map obtained from Landsat (Figure 28), doesn't show any significant overflow from the lava lake.

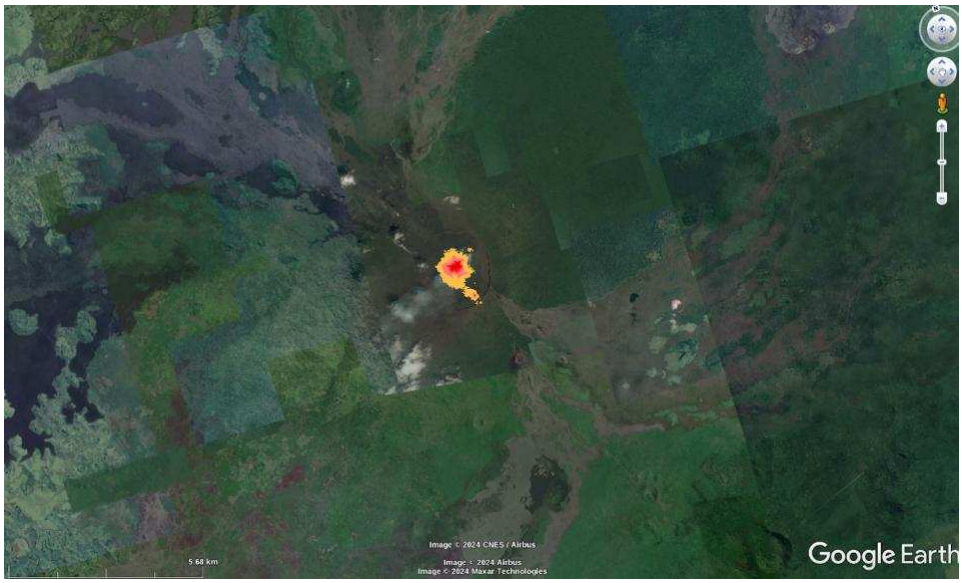

Figure 28. Maps of thermal anomalies derived from the Landsat 8 image (30m spatial resolution) acquired on 28 January 2024 at 20:16 GMT.

References

Boccardo, P., Gentile, V., Tonolo, F. G., Grandoni, D., Vassileva, M. (2015). Multitemporal SAR coherence analysis: Lava flow monitoring case study. 2015 IEEE International Geoscience and Remote Sensing Symposium (IGARSS), 2699-2702, doi: 10.1109/IGARSS.2015.7326370

Oh, J., and C. Lee (2014). Automated bias-compensation of rational polynomial coefficients of high-resolution satellite imagery based on topographic maps, ISPRS J. Photogramm. Remote Sens., 100, 12–22.

Ganci, G., Cappello, A., Bilotta, G., Herault, A, Zago, V., Del Negro, C. (2018). Mapping Volcanic Deposits of the 2011–2015 Etna

Nuth, C. and A. Kääb (2011). Co-registration and biascorrections of satellite elevation data sets forquantifying glacier thickness change, TheCryosphere, 5, 271-290, doi:10.5194/tc-5-271-2011

Ganci G., Cappello A., Bilotta G., Herault A., Zago V, Del Negro C. (2018). Mapping Volcanic Deposits of the 2011–2015 Etna Eruptive Events Using Satellite Remote Sensing, vol. 6, 83, doi:10.3389/feart.2018.00083.

Rupnik, E., Daakir, M., Pierrot Deseilligny, M. (2017). MicMac – a free, open-source solution for photogrammetry. Open geospatial data, softw. stand. 2: 14. doi:10.1186/s40965-017-0027-2.

5.2.4. Synthesis of Nyamulagira activity from late 2022 through 2023

Since 2014, an intermittent lava lake inside the pit crater located within the Nyamulagira caldera has been observed (Campion, 2014; Smets et al., 2014, 2015; Coppola et al., 2016). The eruptive activity increased in March 2023 with several lava overflows from the pit crater, with the lava that reshaped the caldera floor. On the evening of 19 May 2023, a glow was observed above Nyamulagira's caldera from the city of Goma, suggesting a mighty activity. The lava overflowed the caldera rim in the following day, moving along the volcano's western flank. In the GSNL - Virunga Supersite initiative framework, I used SAR images from Sentinel-1 and Cosmo-SkyMed satellites provided by the European Space Agency and the Italian Space Agency, respectively, to analyse the ground deformation during this peak activity (March-May 2023) and map the lava flow extent. Radar images are fundamental to studying the activity of this volcano since it is located in a remote area with limited access, and the cloud coverage of the tropical environment limits the usage of satellite optical images.

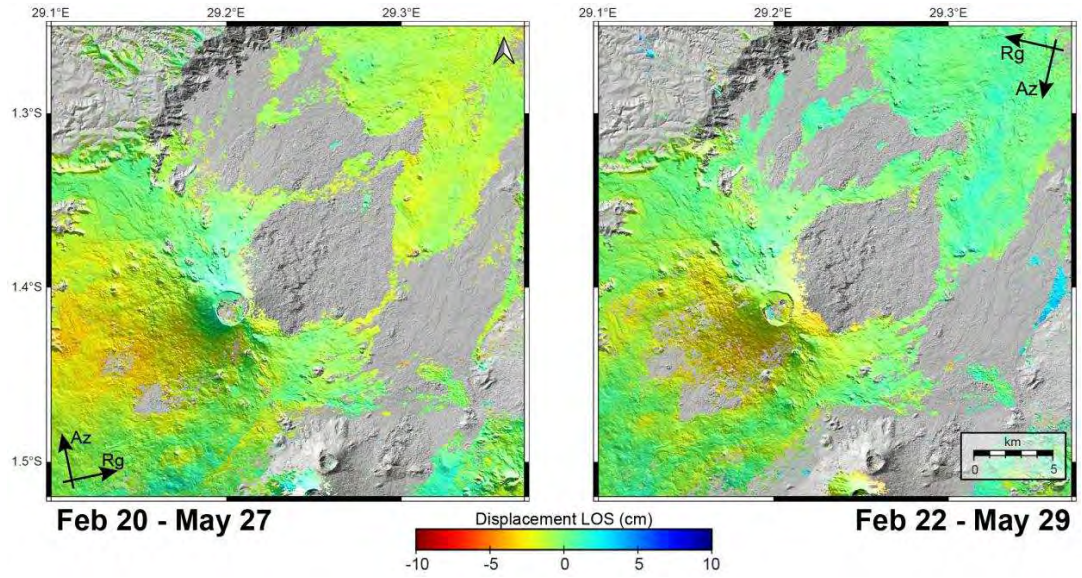

Figure 29. Sentinel-1 deformation maps for the period February-May 2023.

SAR images have been processed using Gamma software (Wegmuller et al., 1998). I evaluated deformation maps for the ascending and descending orbits of the Sentinel-1 satellite using the stacking technique to reduce the noise. To do this, I processed interferograms with a short temporal baseline (12 days between the two acquisitions). The images were multilooked at 13x2 in range and azimuth directions, respectively, to obtain slightly square pixels with a resolution of ~30x30m^2 and reduce the noise. The SRTM 1 arcsec has been used to remove the topographic phase component and geocode the final products. The interferograms have been filtered with an adaptive filter (Goldstein and Werner, 1998).
The minimum cost flow unwrapping algorithm has been used to convert the phase to

deformation. A common reference area, considered stable, has been selected northwest of the caldera. A residual orbital plane has been evaluated and removed. All the final deformation maps have been summed to evaluate the total displacement in the covered period (Figure 29).

Since Cosmo SkyMed SAR images have a higher spatial resolution (namely 2x2m^2), I used the amplitude images to detect and roughly map the lava flow extent (Figure 30). Indeed, the new lava changes the backscat-tering power of the surface. I processed images acquired before and after May 19, 2023, in ascending and descending orbits. The images were multilooked at 3x3 in range and azimuth to obtain ~6x6m^2 pixels. This is the best way to reduce the speckle noise on the amplitude images.

- **Deformation maps**

The Sentinel-1 ascending and descending deformation maps obtained by stacking the interferograms show a signal in range decrease (movement toward the satellite - up to ~3 cm) in a large area southwest of the caldera (Fig. 1). This signal could be consistent with an uplift produced by an inflating deep magma chamber (at ~30km) slightly shifted southwest of the caldera. The presence of a deep source at Nyamulagira was already introduced to explain some far field displacement (e.g. Wauthier et al., 2013). However, the signal-to-noise ratio for the interferograms is low, and this signal could be a residual noise that the stacking technique, with the simple correction applied, couldn't remove (e.g. Biggs et al., 2007). A proper multi-temporal InSAR analysis with the use of a larger number of interferograms with a longer temporal baseline and the use of external data to reduce the atmospheric noise (e.g. GNSS zenith delay or weather models) could improve the results confirming the presence of the uplift. Furthermore, it could provide information on the temporal evolution of the ground deformation that is possibly correlated to the eruptive activity inside the caldera.

- **Lava flow**

The changes in the amplitude of the Cosmo SkyMed images acquired before and after the eruptive episode allowed for roughly mapping the lava flow extent (Fig. 2). The lava overflowed from the pit crater located on the caldera's northern part and started filling the northwestern quadrant. The lava then went over the western edge of the caldera and began to flow along the side of the volcano, covering about 2km.

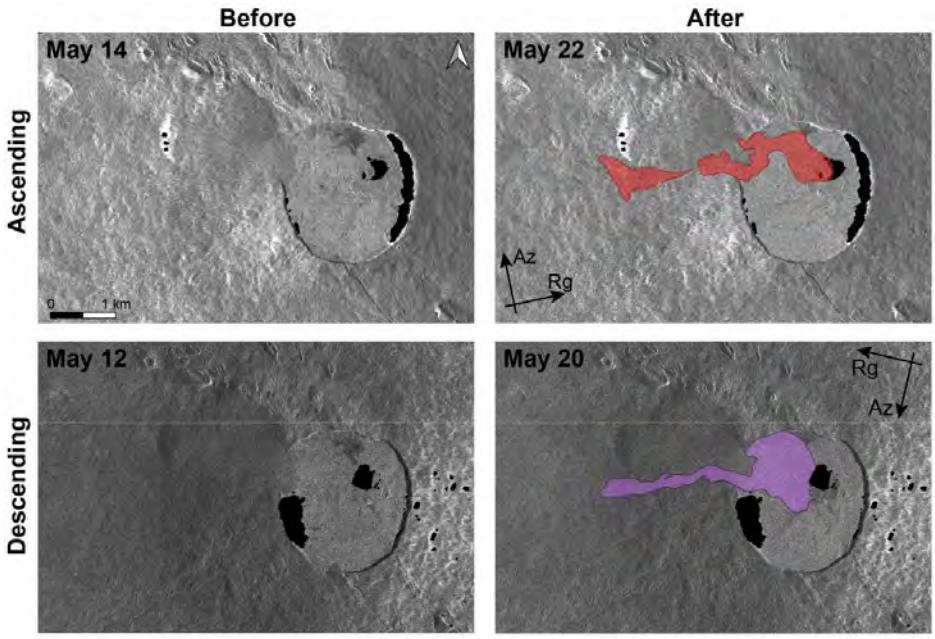

Figure 30. Cosmo skymed amplitude images before and after the lava overflow event.

The differences between the lava extent in the ascending and descending images are related to several reasons, e.g.:

1) the different acquisition times, possibly the lava spread at the tip of the lava flow between May 20 and May 22.

2) the different looking geometries, particularly the incidence angle, produce different reflections that highlight the shape of the lava flow.

3) the entire caldera floor is coated with fresh lava. Indeed, the backscattering power of a two days old lava is comparable to that of a few months old one. Gamma software has masked some pixels (black areas) since they are affected by the shadowing and layover effects (artefacts related to the topography and the incidence angle of the signal).

- **References**

Biggs, J., Wright, T., Lu, Z. and Parsons, B. (2007). Multi-interferogram method for measuring interseismic deformation: Denali fault, alaska Geophysical Journal International 170(3), 1165–1179.

Campion, R. (2014). New lava lake at nyamuragira volcano revealed by combined aster and OMI SO_2 mea-surements Geophysical Research Letters 41(21), 7485–7492.

Coppola, D., Campion, R., Laiolo, M., Cuoco, E., Balagizi, C., Ripepe, M., Cigolini, C. and Tedesco, D. (2016). Birth of a lava lake: Nyamulagira volcano 2011–2015 Bulletin of volcanology 78, 1–13.

Goldstein, R. M. and Werner, C. L. (1998). Radar interferogram filtering for geophysical applications Geophysical research letters 25(21), 4035–4038.

Smets, B., D'Oreye, N. and Kervyn, F. (2014). Toward another lava lake in the virunga volcanic field? Eos, Transactions American Geophysical Union 95(42), 377–378.

Smets, B., Kervyn, M., d'Oreye, N. and Kervyn, F. (2015). Spatio-temporal dynamics of eruptions in a youthful extensional setting: Insights from nyamulagira volcano (dr congo), in the western branch of the east african rift Earth-Science Reviews 150, 305–328.

Wauthier, C., Cayol, V., Poland, M., Kervyn, F., d'Oreye, N., Hooper, A., Samsonov, S., Tiampo, K. and Smets, B. (2013). Nyamulagira's magma plumbing system inferred from 15 years of insar Geological Society, London, Special Publications 380(1), 39–65.

Wegmuller, U., Werner, C. and Strozzi, T. (1998). Sar interferometric and differential interferometric pro-cessing chain IGARSS'98. Sensing and Managing the Environment. 1998 IEEE International Geoscience and Remote Sensing. Symposium Proceedings. (Cat. No. 98CH36174) Vol. 2 IEEE pp. 1106–1108.

5.2.5. Contribution of the satellite monitoring system MOUNTS to the surveillance of Nyiragongo and Nyamulagira volcanoes (DRC)

1. MOUNTS monitoring system

MOUNTS (Monitoring Unrest from Space, www.mounts-project.com, Valade et al. 2019) is a satellite-based volcano monitoring system, exploiting the diversity of sensors on-board the polar-orbiting Sentinel spacecrafts (ESA Copernicus). The synergistic use of radar (Sentinel-1 SAR), short-wave infrared (Sentinel-2 MSI) and ultraviolet (Sentinel-5P TROPOMI) payloads allow for surveillance of surface deformation, emplacement of volcanic deposits, detection of thermal anomalies, and emission of volcanic SO_2 (Figure 31). Deep Learning "plugins" are incorporated to assist specific processing tasks, such as the automatic detection of large deformation (INSAR) and SAR speckle filtering. The system is openly inspired by the MIROVA system (Coppola et al. 2020), whereby volcanic activity is visualized through the systematic display of geo-referenced images and time-series of the above-mentioned parameters at several tens of active volcanoes worldwide.

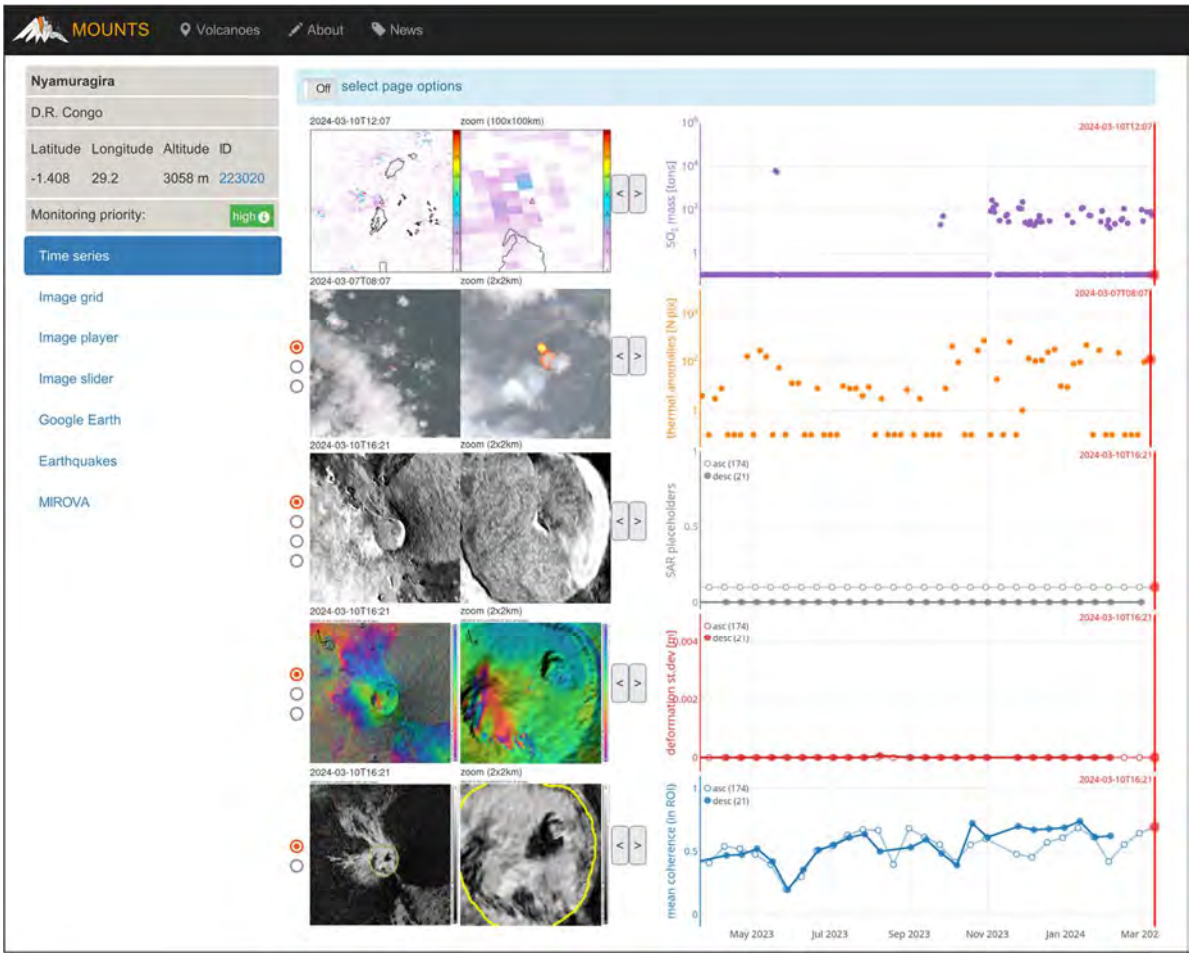

Figure 31. Screenshot of the MOUNTS web interface (www.mounts-project.com) showing the monitoring of Nyamulagira volcano through Sentinel-5P (SO_2 mass in purple), Sentinel-2 (hot pixels in orange, Massimetti et al. 2020), and Sentinel-1 (SAR amplitude in gray, INSAR displacement in red, INSAR coherence in blue).

2. Nyiragongo

The May 2021 eruption of Nyiragongo was followed by a drastic reduction in the SO_2 emissions and thermal anomalies, consistent with the drainage of the summit lava lake (see Virunga Supersite Biennal Report 2020-2021). In the days following the onset, Sentinel-1 SAR images showed a fast collapse of the crater, evidenced by an increased size and depth of the bottom-most pit crater.

Analysis of the Sentinel-1 SAR images allow recovery of the depths variations of both lava lakes and/or pit crater. This is done by measuring the length of the shadow cast by the crater walls in radar geometry, and multiplying it by the cosine of the radar incidence angle (Wadge et al., 2011). The method has been applied to track lava lake level variations at Nyiragongo (Barrière et

al., 2018) and Erta Ale (Moore et al., 2019), and at Nyamulagira it has been applied by MOUNTS to provide variations of the pit-crater floor (Burgi et al. 2021).

Analysis of Sentinel-1 images shows the collapse which occurred in May 2021 following the lava lake drainage (Figure 32). Interestingly, the analysis also shows that after the collapse the crater has to slowly refill, by approximately 69 m between June-2021 and March-2024. Inspection of Sentinel-2 images (Figure 32, inset) suggests that this progressive crater infilling is related to successive episodes of small intra-crater lava flows.

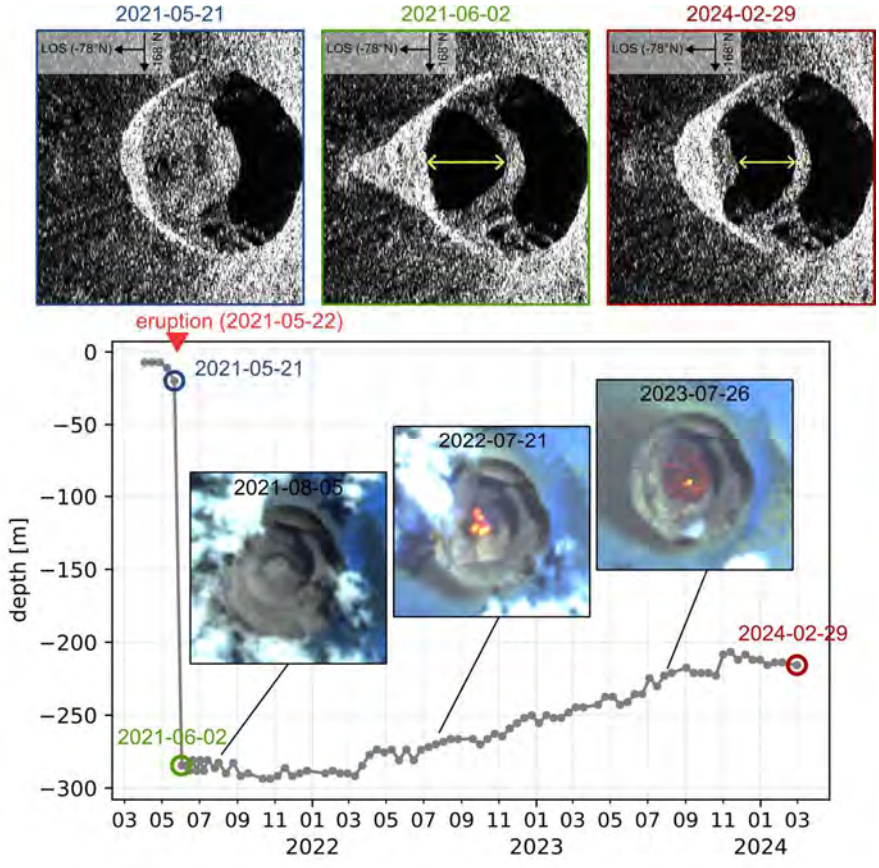

Figure 32. Analysis of Sentinel-1 products (descending orbit) showing the crater collapse in the days following the 2021 eruption onset, and the progressive crater infilling in the following years. Top-most images represent the Sentinel-1 acquisitions displayed in radar geometry, before the eruption onset (2021-05-22), after the onset (2021-06-02), and now (2024-02-29). Yellow arrows indicate the shadow cast by the bottom terrace, where a decrease in shadow width indicates crater infilling. Inset images are Sentinel-2 images (SWIR band composition) which suggest that this infilling is caused by successive lava flows inside the crater.

3. Nyamulagira

Much like the analysis presented for Nyiragongo, analysis of Sentinel-1 SAR images allows recovery of the changes in the floor depth of Nyamulagira's pit crater and main caldera. Both Burgi et al. 2021 and MOUNTS's contribution to Virunga Supersite Biennal Report 2020-2021 showed that during the period 2018-Jan to 2020-June, the pit crater floor at Nyamulagira suffered variations, characterized by a phase of fast collapse (fall of the crater floor in May/June 2016), which was both preceded and followed by phases of slow re-filling (rise of the crater floor). Extending this analysis up to 2024 (Figure 33b), we notice that the pit crater floor suffered similar phases of collapse and refill. In particular, a large collapse episode was observed in May-2021 (~120 m drop), and a second slower collapse was observed in Aug/Nov 2023 (~40 m drop). Following the large collapse episode in May-2021, the inner-pit crater slowly started refilling. Once the pit was completely refilled, lava flows started to emplace onto the main caldera floor, causing a progressive infilling of the caldera and a subsequent decrease of caldera outer wall heights (Figure 33a).

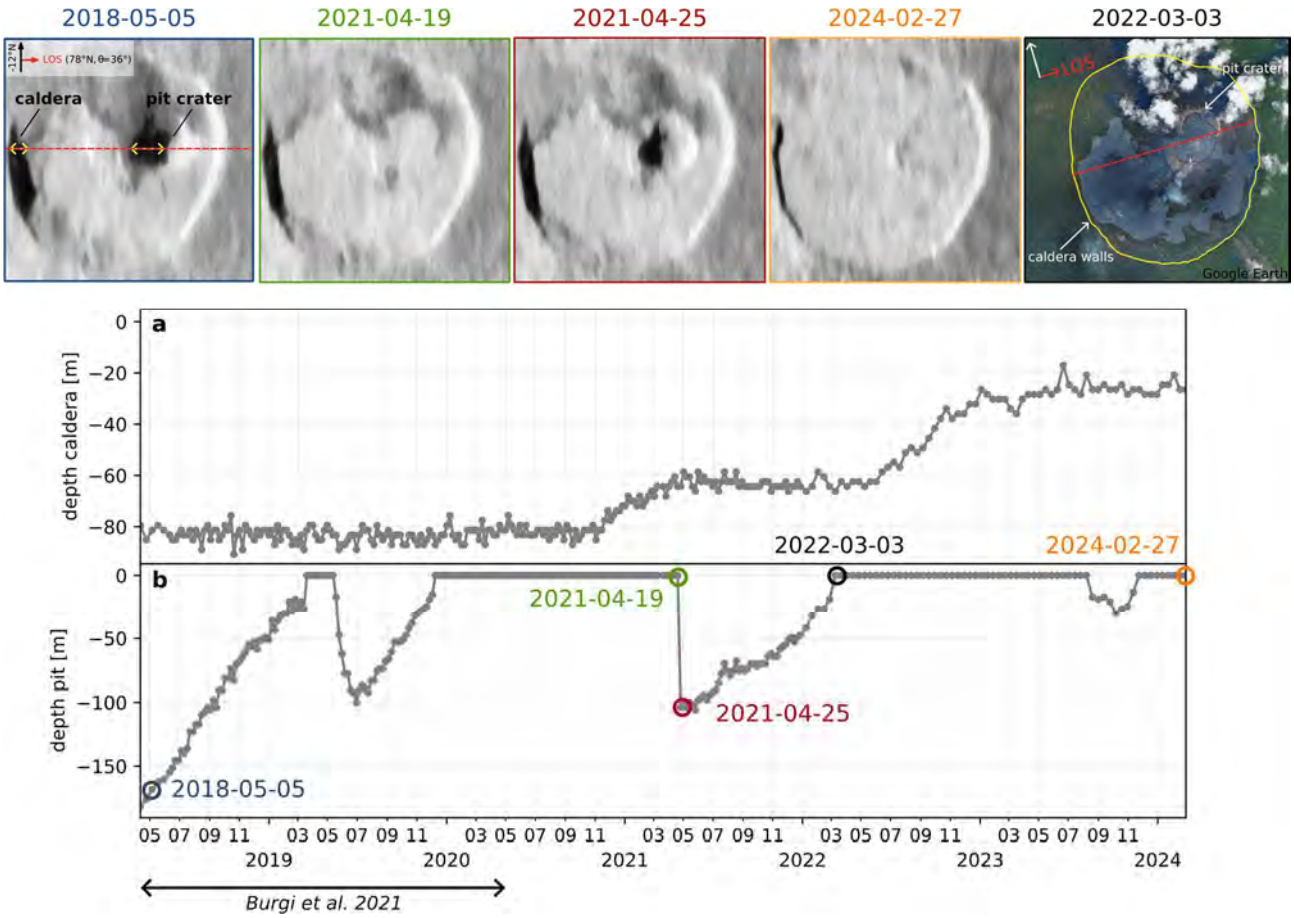

Figure 33. Variations of (a) the main caldera floor and (b) the pit crater floor at Nyamulagira during the period 2018/04 to 2024/03, analyzed by MOUNTS from Sentinel-1 images. Top-row images: Sentinel-1 SAR images (ascending orbit 174) in radar geometry; yellow arrows indicate the SAR shadow used to recover depths of both the caldera floor and pit crater floor along the radar Line of Sight (LOS). Top-row right-most image: high-resolution optical image acquired on 2022-03-03 (Google Earth), dashed red line indicates the radar LOS along which the depths were calculated.

The infilling of the main caldera (Figure 33a) eventually facilitated lava flows to overflow outside the caldera walls onto the western slopes of the edifice, as observed from the INSAR coherence map on 2023-05-29 (Figure 34). During this event, the entire caldera floor was recovered in lava flows, as shown by the decrease in the mean coherence value (Figure 33b, Polcari et al. 2024). This event was associated with the very high SO_2 emissions witnessed on 2023-05-19 (Figure 33a) which emitted ~6 kilotons of SO_2.

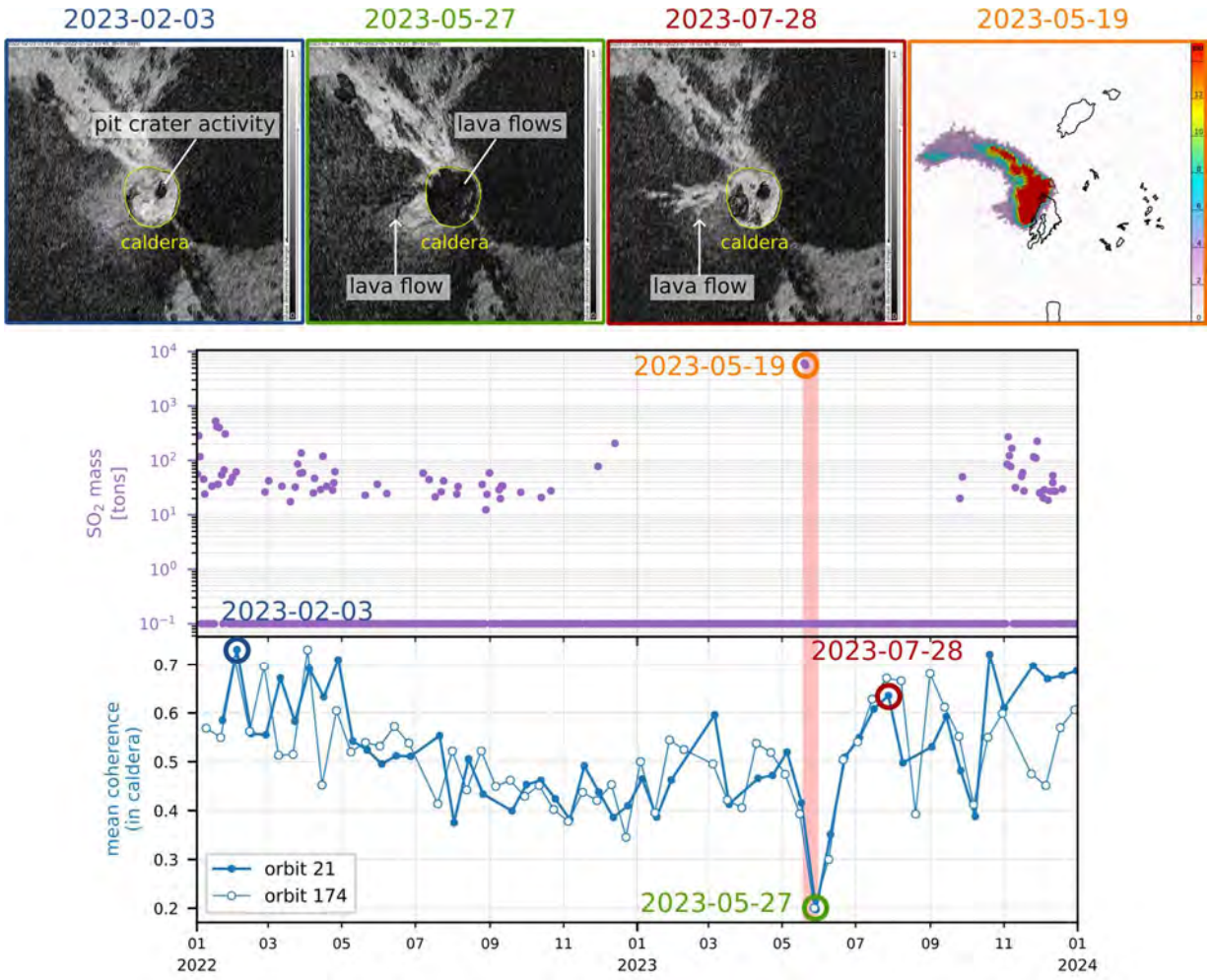

Figure 34. Nyamulagira (a) SO_2 emissions and (b) mean INSAR coherence in the caldera during the period 2022/01 – 2024/01. The caldera area inside which the mean coherence is computed (Polcari et al. 2024) is circled in yellow in the geocoded coherence images (top row).

Fundings

The development of MOUNTS was funded from 2017-2019 by Geo.X (Research Network for Geosciences in Berlin and Potsdam), and between Jan-2021 to Jan-2023 was supported by the UNAM PAPIIT funding (project IA102221).

References

Barrière, J., d'Oreye, N., Oth, A., Geirsson, H., Mashagiro, N., Johnson, J.B., Smets, B., Samsonov, S., Kervyn, F., 2018. Single-station seismo-acoustic monitoring of Nyiragongo's lava lake activity (D.R. Congo). Front. Earth Sci. 6, 82

Biggs, J.; Pritchard, M.E. Global volcano monitoring: What does it mean when volcanoes deform? Elements 2017, 13, 17–22.

Burgi P.-Y., Valade, S., Coppola D., Boudoire G., Mavonga G., Rufino F., and Tedesco D., Unconventional filling dynamics of a pit crater, EPSL, 2021

Coppola D, Laiolo M, Cigolini C, Massimetti F, et al. (2020) Thermal Remote Sensing for Global Volcano Monitoring: Experiences From the MIROVA System. Front. Earth Sci. 7:362. doi: 10.3389/feart.2019.00362

Massimetti, F., Coppola, D., Laiolo, M., Valade, S., Cigolini, C., Ripepe M., Volcanic Hot-Spot Detection Using SENTINEL-2: A Comparison with MODIS–MIROVA Thermal Data Series, Remote Sens., 2020, 12(5), 820

Moore, C., Wright, T., Hooper, A., Biggs, J., 2019. The 2017 eruption of Erta ’Ale volcano, Ethiopia: insights into the shallow axial plumbing system of an incipient mid-ocean ridge. Geochem. Geophys. Geosyst. 20, 5727–5743

Polcari, M., C. Belagizi, E. Ferrentino, S. Valado, D. Coppola, S. Salvi. Analysis of the lava lake and magma flows during 2023 Nyamulagira volcanic activity detected by SAR coherence variations. IAVCEI Cities on Volcanoes, Guatemala, 11–17 Feb 2024

Theys, N.; Hedelt, P.; De Smedt, I.; Lerot, C.; Yu, H.; Vlietinck, J.; Pedergnana, M.; Arellano, S.; Galle, B.; Fernandez, D.; et al. Global monitoring of volcanic SO2 degassing with unprecedented resolution from TROPOMI onboard Sentinel-5 Precursor. Sci. Rep. 2019, 9, 1–10

Valade, S., Ley, A., Massimetti, F., D’Hondt, O., Laiolo, M., Coppola, D., Loibl, D., Hellwich, O., Walter, T.R., *Towards Global Volcano Monitoring Using Multisensor Sentinel Missions and Artificial Intelligence: The MOUNTS Monitoring System*, Remote Sens., 2019, 11, 1528

Wadge, G., Cole, P., Stinton, A., Komorowski, J.-C., Stewart, R., Toombs, A.C., Legendre, Y., 2011. Rapid topographic change measured by high-resolution satellite radar at Soufriere Hills volcano, Montserrat, 2008–2010. J. Volcanol. Geotherm. Res. 199, 142–152

5.2.6. Thermal activity at Nyiragongo and Nyamulagira volcanoes (DRC) detected by the MIROVA system: 2022-2023 report

In this short report I summarize the satellite thermal observations made by the MIROVA system (www.mirovaweb.it) on the Nyiragongo and Nyamulagira volcanoes during 2022-23.

1. **Nyiragongo volcano**:

During 2022-2023, the Nyiragongo heat flux was characterized by an extremely variable pattern with periods of low or totally absent thermal emission, alternating with pulsations characterized by VRP > 100 MW. At least 5 thermal pulses have exceeded 1000 MW during the two-years-long analysed period. This occurred on 5 Jan 2022, 24 Mar 2022, 29 Nov 2022, 16 Mar 2023 and 10 Jul 2023. The impulsive thermal activity seems to be indicative of an open-vent system (typical of lava lakes) not yet well developed. Low thermal emissions are possibly linked to a continuous degassing on the crater floor, alternating with the sporadic resumption of eruptive activity (Strombolian activity? small lava lakes?) which however is not persistent over time. Overall, approximately 1.9×10^{15} J were issued between 2022 and 2023, with a time-averaged VRPmean=29.4 MW.

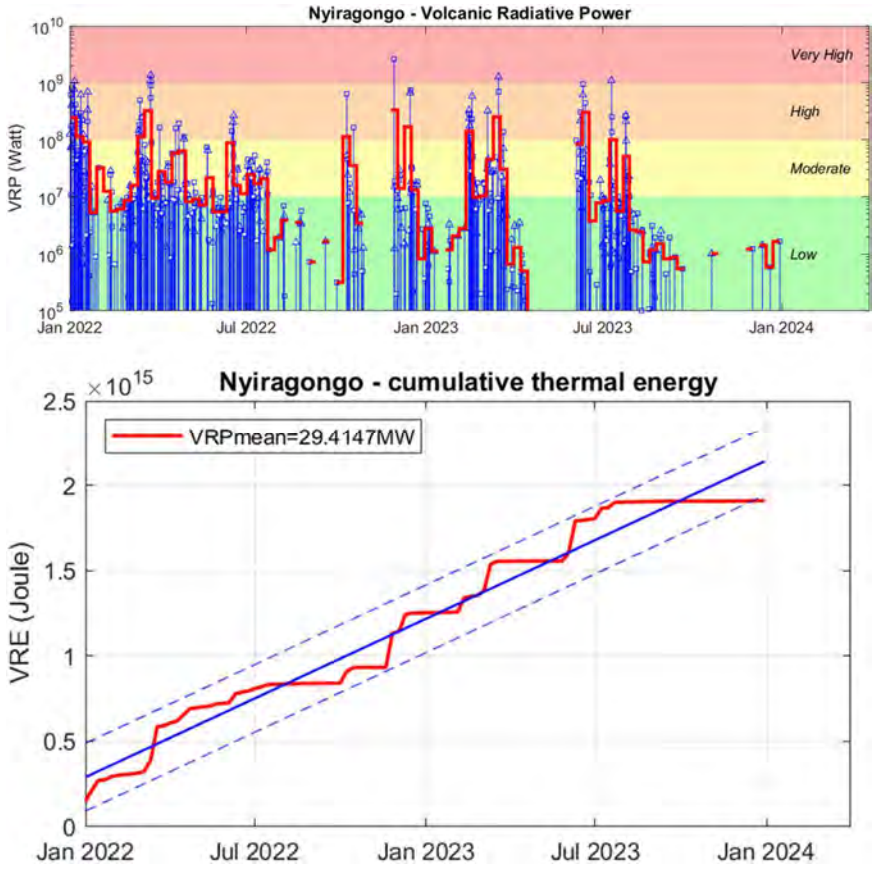

Figure 35. (a) Volcanic Radiative Power (VRP) recorded at Nyiragongo volcano by the MIROVA system during 2022-2023. (b) Cumulative Radiant Energy recorded in the same period.

2. Nyamulagira volcano:

In the period 2022-2023, the thermal activity of Nyamuragira was continuous and persistent, oscillating between moderate (10 MW < VRP < 100 MW) and very high VRP (1000 MW < VRP < 10000 MW). The phase of greatest radiant flux occurred on 19 May 2023 (23:06 UTC) when a VRP=10.6 GW were reached. This phase occurred in correspondence with a lava "overflow" outside the summit caldera extending about 3-4 km on the west flank and fed by an effusion rate of about 30 m3/s (pers. communication to C. Balagizi). The effusive activity vanished in the following hours and emitted approximately ~0.9×10^{15} J. The effusive phase is followed by a period of low thermal activity ending on September 2023. Since then the thermal flux has returned to pre-overflow values. Overall, 4.5×10^{15} J were emitted between 2022 and 2023, with a time-averaged VRP_{mean}= 76.4 MW.

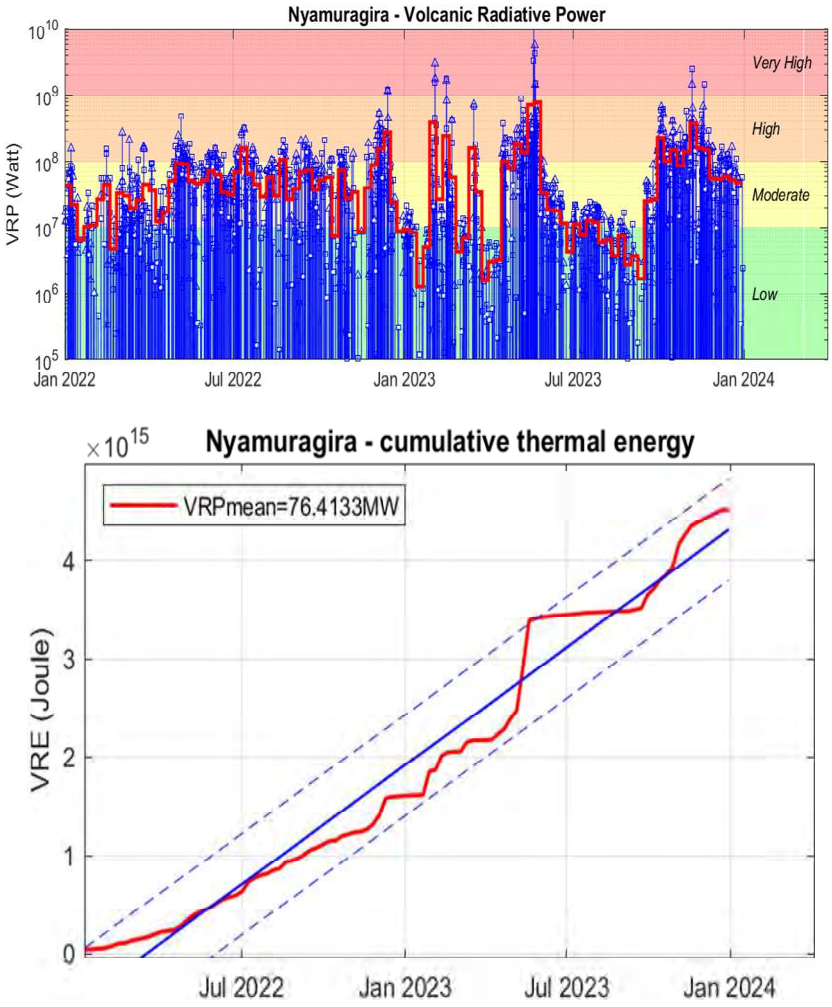

Figure 37. (a) Volcanic Radiative Power (VRP) recorded at Nyamuragira volcano by the MIROVA system during 2021. (b) Cumulative Radiant Energy recorded in the same period.

Publications

Peer reviewed journal articles

Sadiki, A.T., Kyambikwa, A.M., Namogo, D.B. et al. Analysis of the Seismicity Recorded before the May 22, 2021 Eruption of Nyiragongo Volcano, Democratic Republic of the Congo. J. Volcanolog. Seismol. 17, 246–257 (2023). https://doi.org/10.1134/S0742046323700136

Borges D.E. et al. (2023), "Earth observations into action: the systemic integration of earth observation applications into national risk reduction decision structures". Journal of Disaster Prevention and anagement, https://doi.org/10.1108/DPM-09-2022-0186

Cornelis Schwenk, Sophie Negele, Charles M. Balagizi, Werner Aeschbach, Bertram Boehrer (2022) High temperature noble gas thermometry in Lake Kivu, East Africa, Science of The Total Environment, https://doi.org/10.1016/j.scitotenv.2022.155859.

Muvundja Fabrice Amisi, Masilya Pascal Mulungula, Kisekelwa Tchalondawa Kisse, Charles M. Balagizi et al. (2022) Current status and strategic way forward for long-term management of Lake Kivu (East Africa), Journal of Great Lakes Research, 2022, ISSN 0380-1330, https://doi.org/10.1016/j.jglr.2022.04.004

S. Minissale, M. Casalini, C. Cucciniello, Charles M. Balagizi, D. Tedesco, G. Boudoire, V. Morra, L. Melluso, (2022) The geochemistry of recent Nyamulagira and Nyiragongo potassic lavas, Virunga Volcanic Province, and implications on the enrichment processes in the mantle lithosphere of the Tanzania-Congo craton, Lithos, Volumes 420–421, 2022, 106696, ISSN 0024-4937, https://doi.org/10.1016/j.lithos.2022.106696

Charles M. Balagizi, Marcellin M. Kasereka, Albert M. Kyambikwa, Emilio Cuoco, Ilenia Arienzo, Marcello Liotta, characterizing groundwater recharge sources using water stable isotopes in the North Basin of Lake Kivu, East Africa, Chemical Geology, 594, 2022, 120778, ISSN 0009-2541, https://doi.org/10.1016/j.chemgeo.2022.120778

Georges Mavonga Tuluka (Author), Thystere Matondo Bantidi (Author), Arsène Tumaini Sadiki (2023), Volcanic Seismicity for the East Democratic Republic of Congo: Volcanic Hazard for the Eastern DR Congo. LAP LAMBERT Academic Publishing. ISBN-13 : 978-6206159636.

Plisnier P-D, Kayanda R, Obiero K, Vodaceck A, Abegaz H, Achieng A, Akonkwa B, Albrecht C, Balagizi C et al., 2022. Need for a long-term multi-lake harmonized monitoring of African Great Lakes. Accepted for publication in the Journal of Great Lakes Research

Conference presentations/proceedings

M. Polcari, C. Balagizi, E. Ferrentino, S. Valado, D. Coppola, S. Salvi, 2023. Analysis of the lava lake and magma flows during 2023 Nyamulagira volcanic activity detected by SAR coherence variations. In Multi-scale and multi-parametric geodetic monitoring and modeling for studying and forecasting volcanic activity session, COV12, Guatemala

Balagizi, C., Mashagiro, N., Kasereka, M., and Kelly, P.: Pre- and post-eruptive gas composition measurements at Nyiragongo Volcano, East Africa, using a portable Multi-GAS, EGU General Assembly 2023, Vienna, Austria, 24–28 Apr 2023, EGU23-16823, https://doi.org/10.5194/egusphere-egu23-16823, 2023.

Charles M. Balagizi, Ganci, G., Trasatti, E., Tolomei, C., and Beccaro, L.: The 2021 Nyiragongo (DR Congo) eruptive crisis monitored by multi-sensor satellite remote sensing data, EGU General Assembly 2022, Vienna, Austria, 23–27 May 2022, EGU22-12586, https://doi.org/10.5194/egusphere-egu22-12586, 2022.

Balagizi C, 2023. Volcanology in the Democratic Republic of the Congo, Focus on Volcano Monitoring and Volcano Hazards in the Virunga Volcanic Province. 1st International Workshop for African Volcanologists July 24-27, 2023; Nyeri-Kenya

Research products

The main research products of the Virunga Supersite for the period from January 2020 to December 2021 are included in the present report. Thus, they will be accessible via the link to the report which will be available once the report has been approved; the report will also be available at the GEO GNSL website, Virunga Supersite section at http://geo-gsnl.org/supersites/permanent-supersites/virunga-supersite/ . However, there is a plan to open a website for the Virunga Supersite which will help to share the research products.

Type of product	Product provider	How to access	Type of access
Map of the seismicity recorded before the May 22, 2021 Eruption of Nyiragongo Volcano	***Mavonga C, Kyambikwa A & Sadiki (OVG)***	*Supersite coordinator or scientists who produced the map*	*Public*
Updated map of fractures created by the Nyiragongo 2021 eruption and the seismicity that followed the eruption	***Ciraba H, Iragi K, Kavuke J., NZamu S, Balagizi C (GVO)***	*Supersite coordinator or scientists who produced the map*	*Limited to GSNL scientists*
Updated Data of Lake Kivu Physico-chemical composition	***Balagizi C & Kasereka M (GVO)***	*Supersite coordinator or GVO*	*Limited to GSNL scientists and later on to the Public after publication in scientific journal*
High temperature noble gas thermometry in Lake Kivu	***Cornelis Schwenk, Sophie Negele, Charles M. Balagizi, Werner Aeschbach, Bertram Boehrer***	***doi.org/10.1016/j.scitotenv.2022.155859***	***Contact authors, GVO***
Data related to air quality at Lake Kivu surface	***Balagizi C, Kasereka M & Mashagiro N (GVO),***	*Supersite coordinator or scientists who produced the map*	*Limited to GSNL scientists*
Geochemistry data of recent Nyamulagira and Nyiragongo potassic lavas	***GVO and patners***	*GVO, Supersite coordinator or partners with whom the data was produced doi.org/10.1016/j.lithos.2022.106696*	*Contact authors, GVO*
Sable isotopes of water of rivers of the Virunga and Lake Kivu	***Balagizi C, Kasereka M (GVO),***	*https://doi.org/10.1016/j.chemgeo.2022.120778*	*Public*

Research product issues

All the research products are not open to the public; some are still under embargo to allow the scientific team to publish their results. However, the results are fully open for hazards assessment and crisis managements, but can be accessed on request.

6. Dissemination and outreach

- Scientific products were already sent to local institutions that are involved in hazards assessment, particularly the GVO that monitors the Nyiragongo and Nyamulagira active volcanoes.
- The Virunga Supersite has a logo which is shown below:

Training of local scientists:

1°) Albert Kyambikwa, a GVO Junior researcher working in the department of semiology, has finished his two years masters in Volcanology at the University at Buffalo with thesis focusing on the Reconstruction and modeling of lava rheology at Nyiragongo Volcano.

2°) Arsène Tumaini Sadiki, a GVO Junior researcher working in the department of semiology, has finished 18 months training in volcano seismology at Istituto Nazionale di Geofisica e Vulcanologia (INGV), Osservatorio Etneo - Sezione di Catania; Italy

3°) Olivier Munguiko Munyamahoro, a GVO Junior researcher working in the department of semiology, participated in a short-term scientific training at the Center for the Study of Active Volcanoes; an International Training Course in Volcano Hazards Monitoring. The was held at Hilo campus – University of Hawaii in partnership with the Hawaiian Volcano Observatory, and second part in Vancouver, Washington at the USGS Cascades Volcano Observatory. This training was fully funded by the USGS's Volcano Disaster Assistance Program (VDAP-USAID).

4°) Marcellin Kasereka, a GVO Junior researcher working in the department of Geochemistry, is the second year of a master in analytical chemistry focusing on fluids (gases and waters) at the University of Burundi, in Burundi.

5°) MOSANGE Thérèse from University of Goma is having a 2 years masters in Environmental Sciences at Abomey Calavi University (Benin), with a scholarship from Abomey Calavi.

7. Funding

The Virunga Supersite has no funding; all the activities were realized by scientists working on a voluntary basis.

8. Stakeholders interaction and societal benefits

The Goma Volcano Observatory (GVO) remains the main and direct beneficiary of the Virunga Supersite services and products. In fact, most of the products are science related and in direct link with volcano study and monitoring. The products are entirely integrated in the routine of the GVO that produces the information to communicate to stakeholders, such as the weekly bulletin about volcano eruptive level, and other communication that is directed to the government and the population.

9. Conclusive remarks and suggestions for improvement

AThe Virunga Geohazards Supersite is presently well established and an operating scientific group formed of local and international scientists and agencies. We expect to get fundings that will allow this motivated team to get instruments for ground-based data collection, local infrastructure development and for the training of the local scientists.

10. Dissemination material for CEOS (discretionary)

Please refer to section 5.